STRENGTHENING POTENTIAL OF SINGLE-WALLED CARBON NANOTUBES IN PHENOLIC RESIN COMPOSITES

by

BRITTANY CLAIRE KERR
B.S. University of Washington, 2004

A thesis submitted in partial fulfillment of the requirements
for the degree of Master of Science
in the Department of Materials Science and Engineering
in the College of Engineering and Computer Science
at the University of Central Florida
Orlando, Florida

Spring Term
2010

ABSTRACT

Strengthening potential of single-walled carbon nanotubes (SWCNTs) in a phenolic resin composite was evaluated by characterization of purified and phenyl sulfonated SWCNTs, investigation of the load transfer capability of the purified SWCNTs, and characterization of the composites. Purified and phenyl sulfonated SWCNTs, as well as their composites, were examined by Raman spectroscopy, thermogravimetric analysis, scanning electron microscopy equipped with energy dispersive spectroscopy, transmission electron microscopy, X-ray photoelectron spectroscopy and ultra violet-visible spectrometry. Fabrication of the SWCNT/phenolic resin composite was performed by first dispersing the SWCNTs in ethylene glycol and then homogenizing the mixture with phenolic resin. The ethylene glycol was then evaporated from the mixture and the SWCNT/phenolic resin composite was cured at 200°C for 1 hour. The dispersion of SWCNTs in the phenolic resin was reduced with higher SWCNT concentrations. Load was transferred from the phenolic resin to the purified SWCNTs. This demonstrated the potential to strengthen phenolic resin composite with SWCNT reinforcement. The load transfer efficiency in total tension (0.8%) decreased with an increase in SWCNT concentration, while in total compression (-0.8%), the load transfer efficiency remained constant. At very low strain (± 0.2%), the load transfer efficiency remained constant regardless of SWCNT concentration in both tension and compression. Characterization of the phenyl sulfonated SWCNTs indicated that calcium was introduced as a contaminant that interfered with functionalization of the SWCNTs. The use of contaminated phenyl sulfonated SWCNTs resulted in macroscopic inhomogeneity within the composite.

ACKNOWLEDGMENTS

I would like to thank my advisor, Yongho Sohn, for his guidance and support throughout the research process. Additional thanks go to the members of the thesis committee, Kevin Coffey and Linan An. I would also like to express my appreciation to Brad Files and the entire NASA Johnson Space Center nanomaterials group for allowing me the use of their laboratories and providing the materials needed for this research. I'd like to extend a special thanks to Peter J. Boul for purifying and functionalizing the nanotubes that were used on this project, Padraig G. Moloney for acquiring TEM micrographs and TGA analysis, Edward Sosa for performing XPS analysis, and James E. Martinez and Shakira Morera-Felix for their laboratory equipment support. Additionally, I would like to thank Padraig G. Moloney, Edward Sosa, and Pavel Nikolaev for the technical expertise and recommendations they provided.

TABLE OF CONTENTS

LIST OF FIGURES

LIST OF ACRONYMS

CNT	Carbon nanotube
DMF	Dimethyl formamide
EDS	Energy dispersive spectroscopy
EG	Ethylene glycol
FEG	Field emission gun
HiPco	High-pressure CO (carbon monoxide)
IPA	Isopropyl alcohol
LCA	Lightweight carbon ablator
MMOD	Micrometeoroid and orbital debris
MWCNT	Multi-walled carbon nanotubes
PICA	Phenolic impregnated carbon ablator
PVA	Poly (vinyl alcohol)
RBM	Radial breathing mode
RLT	Raman load transfer
SWCNT	Single-walled carbon nanotube
SEM	Scanning electron microscope
TEM	Transmission electron microscope
TGA	Thermogravimetric analysis
UV-VIS	Ultra violet-visible
XPS	X-ray photoelectron spectroscopy

DEFINITIONS

Nanotubes	This is a general term to refer to nanotubes in any form, whether isolated, bundled, clustered, or agglomerated.
Bundle	Due to van der Waals forces between each nanotube, *a bundle* consisting of several to hundreds of aligned nanotubes can form. Physically they would appear as a rope woven from many fibers (individual nanotubes).
Cluster	Clusters are made up of many tangled, tightly bound nanotube bundles without any preferred alignment.
Dispersion	Dispersion refers to separation of bundles from clusters and isolating nanotubes from bundles, in a solution. Perfect dispersion is the isolation of all individual nanotubes. However, in this study, “good dispersion” refers to a solution where most nanotubes are separated into bundles and possibly some isolated nanotubes. In this case a minimum cluster size should not exceed 25µm.
Agglomeration	Nanotubes that are dispersed in solutions should be homogeneously mixed, meaning that isolated nanotubes, bundles, and clusters less than 25µm in size are uniformly distributed throughout the solution. However, over time, the nanotubes, bundles, and clusters tend to *agglomerate,* or collect into large, loosely packed groups. This causes selected areas within the solution (and fabricated composite) to be depleted of any carbon nanotubes.

1 INTRODUCTION

Carbon nanotubes (CNTs) were discovered in 1991 and show great promise for many applications. CNTs can be visualized as a single layer of graphene rolled into a seamless tube. Single-walled carbon nanotubes (SWCNTs) are formed by a single tube of graphene, while multi-walled carbon nanotubes (MWCNTs) are made up of concentric tubes of graphene. CNTs have been shown to exhibit very high strength and Young's Modulus. They also have a high aspect ratio.

CNT composites are of particular interest for strengthening NASA's current heat shields. During Earth reentry, spacecraft are exposed to extreme heating conditions. It is essential to protect these spacecraft and payload from hot gases during reentry and much research has gone into the development of such heat shields. One type of heat shield is the lightweight carbon ablator (LCA), which protects the vehicle by slowly burning away in order to carry heat away from the vehicle (Tran, et al., 1997).

Phenolic impregnated carbon ablator (PICA) is a specific type of LCA, which has been developed at Ames Research Center, San Jose, CA. It consists of a preformed carbon fiber substrate, infiltrated with phenolic resin (Tran, et al., 1997). It was employed on the Stardust heat shield and is considered for the Orion heat shield. PICA displays excellent thermal/ablative properties, oxidation resistance, and low density; however it is intrinsically brittle, which leads to concerns about mechanical strength (Tran, et al., 1997). During planetary missions the heat

shield will be exposed to micrometeoroid and orbital debris (MMOD) impacts, high deflections, and high shear stresses during heat loading.

NASA is currently investigating the incorporation of CNTs into phenolic resin, which could be used in the fabrication of PICA to increase the mechanical strength. The research involves material classification of the phenolic resin composite with 0.25 wt% CNT loading. Samples are evaluated using mechanical testing such as dynamic mechanical analysis and tensile testing. In addition, Raman spectroscopy is used to study stress transfer within the composite and optical and electron microscopy are used to evaluate the CNT dispersion within the composite.

NASA's current research plan uses a CNT concentration of 0.25 wt% for all composite test coupons. Previous CNT research at the NASA Materials Lab has used 0.25 wt% CNTs in other matrix materials and has found, qualitatively, that this concentration yields excellent dispersion and increase in mechanical strength without increasing the viscosity. This same concentration was chosen for the phenolic resin based on past experience/success and allows for comparison with historical data.

The purpose of this study was to examine the characteristics of commercially available HiPco SWCNTs after soft-bake purification and phenyl sulfonation. The load transfer capability of purified SWCNTs in phenolic resin composite was investigated as a function of SWCNT loading and to demonstrate the strengthening potential of SWCNTs. In addition, the influence of

contamination from functionalization of SWCNTs was examined with respect to macroscopic homogeneity.

2 LITERATURE REVIEW

CNTs were first observed in by Iijima (1991) using transmission electron microscopy (TEM). These nanotubes consisted of multiple layers of concentric tubes, called multi-walled carbon nanotubes (MWCNTs). In 1993, SWCNTs were discovered by Iijima and Ichihashi (1993).

2.1 Nanotube Characteristics

SWCNTs can be visualized as a single layer of graphene rolled into a seamless tube (Dresselhaus & Avouris, 2001). Depending on the orientation (or chirality) of the graphene sheet with respect to the nanotube axis, the nanotubes can take on different characteristics such as metallic or semiconducting (Dresselhaus & Avouris, 2001). Carbon nanotubes have a high aspect ratio with a diameter on the order of a few nanometers and length up to the millimeter range (Hata, Futaba, Mizuno, Namai, Yumura, & Iijima, 2004).

2.1.1 Mechanical Properties

CNTs have been shown to exhibit strengths as high as 63 GPa (Yu, Lourie, Dyer, Moloni, Kelly, & Ruoff, 2000) with Young's Modulus greater than 1 TPa (Wong, Sheehan, & Lieber, 1997). Despite having such a high Young's Modulus, CNTs are not brittle, exhibiting very high strains before breaking. Yu et al. (2000) found that the tensile strains required to break CNTs can reach above 5%. However, Cronin, et al. (2004) found that at strains greater than 1.65%, breakage of an isolated nanotube occurred. Cronin, et al. (2004) also found that, even up to the breaking

strain of 1.65%, the nanotube had exhibited elastic deformation and, over a period of time, the two pieces of the severed SWCNT returned to their original combined length.

2.1.2 Electrical Properties

Both metallic and semiconducting nanotubes exhibit unique electrical properties. Because of the near 1-dimensionality of CNTs, scatter of charge carriers during conduction is minimal (Coleman, Khan, Blau, & Gun'ko, 2006). Metallic CNTs display ballistic conduction due to having minimal defects and backscattering (Jorio, Dresselhaus, & Dresselhaus, 2008). MWCNTs have been shown to carry current at densities greater than 10^9 A/cm^2 at temperatures up to 250°C without adverse effects (Wei, Vajtai, & Ajayan, 2001). Semiconducting CNTs have band gaps on the order of 1 eV that varies depending on the chirality and diameter of the CNT (Jorio, Dresselhaus, & Dresselhaus, 2008).

2.2 Applications

Since their discovery nearly two decades ago, CNTs have been heavily studied for a wide array of applications that exploit their mechanical and electrical properties. CNTs are being examined for potential applications in areas such as displays, sensors, energy-storage devices, biomedical devices, and reinforcement for composites. Obraztsov et al. (2000) were able to create a thin film material consisting of aligned CNTs that can carry an emission current density greater than 50 mA/cm^2. This material has possible applications in displays. A field-emission diode prototype fabricated from a CNT/epoxy composite exhibited a uniform field emission and well lit, controllable pixels leading to possible applications in flat panel displays (Wang, Setlur,

Lauerhaas, Dai, & Seelig, 1998). In the electronics industry, isolated CNTs can perform as quantum wires (Tans, et al., 1997). Du, Yeh, & Pan (2005) found that a thin film formed by MWCNTs could be used for supercapacitors with a high power density of 30 kW kg^{-1}. In the biomedical area, CNTs are being explored as a drug delivery agent that can be used for in vivo cancer therapy (Liu, Sun, Nakayama-Ratchford, & Dai, 2007).

2.3 Nanotubes in Polymer Matrix Composites

CNTs have been heavily researched as a strengthening reinforcement in polymeric composites. This application shows promise because of the excellent mechanical strength of CNTs and their high aspect ratio that offers a large interfacial contact area with the composite matrix.

2.3.1 Added Strength

Ryan et al. (2007) found that 0.1 vol% of SWCNTs improved the Young's Modulus of poly(vinyl alcohol) (PVA) by a factor of three and improved the tensile strength by a factor of two. Yeh, Tai, & Liu (2006) found that, in a MWCNT/phenolic resin composite, the tensile strength and Young's Modulus increased with the CNT content; at 4 wt% they were improved by about 65% and 47%, respectively. Despite the impressive array of mechanical properties, much of the research on CNT composites has produced results that fall well short of the theoretical results, primarily due to a lack of CNT dispersion within the matrix (Coleman, Khan, Blau, & Gun'ko, 2006).

2.3.2 Dispersion

Dispersion of reinforcement within the matrix is a key to successful mechanical strengthening of the composite material. An increase in CNT dispersion generally corresponds to an increase in strength and modulus (López Manchado, Valentini, Biagiotti, & Kenny, 2005). Carbon nanotubes are initially closely packed into bundles, which are further entangled into large clusters (Vaisman, Wagner, & Marom, 2006), (Huang & Terentjev, 2008). Due to the large surface area of CNTs, the van der Waals interactions between them is quite strong, making it difficult to disperse them in solutions (Vaisman, Wagner, & Marom, 2006). The attraction must be overcome, which can often be done to some degree by mechanical mixing; however, the solution may not be stable and agglomerations can occur, particularly at higher CNT loadings where CNTs are in closer proximity and able to interact with each other (Huang & Terentjev, 2008).

2.3.2.1 Mechanical Dispersion Methods

Since unmodified CNTs are insoluble in most solvents, mechanical dispersion of the CNTs has been investigated. The most common methods of mechanically dispersing CNTs in solution are ultrasonication and high shear mixing. Ultrasonication has been demonstrated to disperse CNTs fairly well, regardless of the viscosity of the polymer (Huang & Terentjev, 2008); however, there is also evidence that suggests that ultrasonication causes damage and breakage of CNTs (Martinez, et al., 2003). High shear mixing has been used with good dispersion results in viscous mediums with less damage to the CNTs (Huang & Terentjev, 2008).

2.3.2.2 Dispersion Improvement by Alteration of Surface Energies

The dispersibility of CNTs can be improved by surface modification, dispersion in solvents (solution processing) and use of surfactants to improve the solubility of CNTs in a polymer medium when used in conjunction with mechanical mixing. These tactics alter surface energies between CNTs and the solution to improve dispersion and reduce the occurance of agglomeration (Terentjev, 2005). Solution processing is a common method for improving dispersion. In this method the CNTs are dispersed in a solvent that has greater CNT solubility than the matrix polymer. The CNTs and solvent are then mixed with the polymer and the solvent is subsequently evaporated out. This method can be used alone or improved by using a surfactant. The surfactant is used to wrap the individual nanotubes in a cylindrical micelle which then allows dispersion of the CNTs in aquaeous or polar solvents (Vaisman, Wagner, & Marom, 2006). This process requires the use of sonication or high shear mixing. Surface modification, or functionalization, is done by covalently bonding molecules to the side walls of CNTs. This lowers the attractive forces between CNTs causing bundles to be more weakly bound. It also improves the attraction between CNTs and the polymer matrix, encouraging greater dispersion within the uncured medium and reduces the ocurrance of agglomeration. CNTs that were functionalized with PVA molecules were found to be soluble in polar solutions allowing for improved dispersion in the final composite material (Lin, Zhou, Fernando, Liu, Allard, & Sun, 2003). Functionalization has also been shown to increase the bond strength between the CNTs and polymer matrix.

2.3.3 CNT/Matrix Interface

2.3.3.1 Interfacial Bonds

Liao and Li (2001) suggest that the most likely method of load transfer between the polymer matrix and non-functionalized CNTs is by a combination of van der Waals and electrostatic forces as well as mechanical interlocking caused by the difference in coefficients of thermal expansion between CNTs and the polymer matrix. There is very little evidence that strong bonds exist with non-functionalized SWCNTs that would allow greater load transfer. It is believed that in the case of nanotube bundles, the polymer matrix can actually infiltrate the bundle, interlocking with individual nanotubes (Schadler, Giannaris, & Ajayan, 1998) thus allowing load transfer to inner nanotubes within the bundle.

2.3.3.2 Interfacial Structure of the Matrix Material

There are many findings that suggest that, in the vicinity of reasonably well dispersed CNTs, some polymer matrix materials form a structure that differs from that of the bulk matrix material. Ryan et al. (2007) demonstrated that CNTs served as a nucleation site for crystallization of PVA. The PVA was found to be in crystalline form in the near vicinity of CNTs, differing from the structure of the bulk material. It was suggested that the crystalline PVA served as a more significant strengthening mechanism than the CNTs themselves (Coleman, et al., 2006), (Ryan, et al., 2007). Potschky, Fornes, & Paul (2002) observed that polycarbonate had adsorbed to the surface of CNTs creating a layer that differed in crystal structure from the bulk material. This layer was left coating the CNTs after pullout from the matrix due to fracture of the composite;

however, Potschky, Fornes, & Paul (2002) did not observe this effect in a similar CNT composite fabricated with a polyamide-6 matrix. Ding et al. (2003) also observed that CNTs, which had pulled out of the matrix after fracture of the composite, were coated in a layer of polycarbonate.

2.3.4 Test Method for Strengthening Capabilities of CNTs in Composite

Raman load transfer testing can be performed to determine whether load is transferred from the matrix to the filler material in a CNT composite. The degree of load transfer to CNTs from the matrix provides an indication of the strengthening potential of the composite due to the integration of CNTs. Load transfer can be determined by the shift of the G^+ peak of the Raman spectra as a function of strain.

Cronin et al. (2004) performed Raman load transfer on an isolated SWCNT and found that the G^+ peak shifted 14.8 cm^{-1} due to a tensile strain of 0.53%. If it is assumed that the relationship between strain and G^+ peak shift is linear, then this equates to a downshift of 27.92 cm^{-1}/% strain. Therefore, this is the value that could be expected if 100% load transfer is achieved in a composite with CNTs that are aligned with the direction of strain. If CNTs are randomly oriented in a plane, then on average the strain imposed on the CNTs should be factored by the average of cosines, or $2/\pi$ (0.636), resulting in a value of 17.8 cm^{-1}/% strain on the matrix.

3 EXPERIMENTAL PROCEDURE

3.1 Nanotube Synthesis

There are several techniques that can be used to produce CNTs, including carbon arc, laser ablation, chemical vapor deposition, and carbon monoxide disproportionation (Arepalli, et al., 2004). All of these methods leave impurities in the CNTs in the form of metal catalysts and other carbon compounds, including amorphous carbon and fullerenes. Further processes have been developed to remove much of these impurities including boiling in hot water, slow oxidation in air, hot acid digestion, extensive ultra-sonication, centrifugation, and annealing (Arepalli, et al., 2004). In addition to purification, it has been found that surface modification can improve the dispersion of CNTs in polymer composites.

The SWCNTs obtained for this research were produced at Rice University using a gas-phase disproportionation process known as HiPco, which stands for high-pressure carbon monoxide. The HiPco SWCNTs were purified at Johnson Space Center (JSC) using a process called soft-bake, and subsequently functionalized with phenyl sulfonate molecules.

3.1.1 HiPco Process

HiPco is a SWCNT production process that has been shown to produce relatively pure SWCNTs with typically less than 7 mol % iron impurities. The SWCNTs provided for this study were produced at Rice University using the procedure described by P. Nikolaev (2004). The HiPco process uses a high temperature flow of carbon monoxide (CO) to nucleate and grow SWCNTs

on iron catalyst clusters. The first step in the process is to form the metal catalyst by quickly mixing iron pentacarbonyl ($Fe(CO)_5$) and CO at high temperature and pressure. This causes the $Fe(CO)_5$ to decompose and Fe atoms begin to nucleate and grow into small clusters. Carbon atoms from the CO gas nucleate on the iron clusters and begin to grow, forming SWCNTs through the Boudouard reaction:

$$CO + CO \xrightarrow{Fe} CO_2 + C_{(SWCNT)} \quad (1)$$

During the SWCNT growth, the iron clusters continue to grow simultaneously. At larger iron cluster sizes, carbon deposition onto the catalyst is favored over nanotube growth and the process terminates. The final product is a material containing SWCNTs with approximately 7 mol % impurities of iron catalyst (Nikolaev, 2004).

3.1.2 Purification Process

Raw HiPco SWCNTs contain about 7% iron, most of which is coated in a thin shell of amorphous carbon. The soft-bake purification process described by Chiang et al. (2001) was performed at NASA-JSC. The process first causes a breaking of the carbon shell and then removal of the iron and amorphous carbon. In the first step, the raw HiPco SWCNTs are exposed to a wet argon (80%)/oxygen (20%) gas at a temperature of 225°C for 18 hours. This causes some of the iron to oxidize, resulting in a volume increase which breaks the carbon shell. With

the iron exposed, the material is then sonicated in a concentrated hydrochloric acid (HCl) solution which extracts the iron as well as some amorphous carbon.

3.1.3 Functionalization Process

After purification of the HiPco SWCNTs, the functionalization process can be performed to bond phenyl sulfonate molecules to the SWCNTs. This process was developed (Boul, 2008) and performed at NASA-JSC.

The functionalization of the SWCNTs with phenyl sulfonate molecules was carried out in two steps: phenyl groups were bonded to the sidewalls of the SWCNTs, followed by attachment of sulfite molecules to the phenyl groups. In the first step, benzene was added to the SWCNTs and homogenized, followed by the addition of benzoyl peroxide. The mixture was then homogenized at elevated temperature, causing phenyl groups to attach to the sidewalls of CNTs. The phenylated SWCNTs were then rinsed in preparation of the sulfonation phase.

In the second step, the phenylated SWCNTs were mixed with sulfuric acid at elevated temperature. This causes the attachment of sulfite molecules to the phenyl groups on the SWCNT sidewalls. The SWCNTs are then cooled and rinsed with oleum, followed by a sodium hydroxide soak. The CNTs were then rinsed with deionized water until the pH was neutral.

3.2 Composite Fabrication Process

The composite fabrication process was developed by the nanotube group at NASA JSC to prepare a composite material made up of 0.25 wt % CNTs with phenolic resin matrix. It employs the solution processing method and high shear mixing for dispersion of the SWCNTs. The cure cycle is based on recommendations from the phenolic resin manufacturer. This process was used to fabricate the composite test coupons as well as the Raman load transfer (RLT) test specimens.

Phenolic Resin Preparation: 40 g Hexion SC-1008 Phenolic resin was degassed at 65°C under vacuum until 10% mass had been evaporated (approximately 3 hours). This 10% by mass is the isopropyl alcohol (IPA) used to reduce the viscosity of the starting material.

Mold Preparation: The mold, which is 95 mm length by 90 mm width by 8 mm depth, was cleaned with acetone and then sprayed with silicon mold release (Dow Corning 316 Silicon release). The silicon mold release was cured at 230°C for 1 hour.

Dispersion of SWCNTs in EG: A covered beaker with 20 g of EG and 100 mg (for 0.25 wt% SWCNT) of SWCNTs was mixed using a high shear homogenizer at a speed of 20,000 rpm for 1.5 hours. Since it is difficult to disperse the nanotubes directly in phenolic resin, they were first dispersed in EG. The EG is eventually evaporated from the mixture prior to curing of the phenolic resin.

Homogenization of SWCNTs, EG, and phenolic resin: The homogenized SWCNTs/EG was added to the degassed phenolic resin and mixed in a high shear homogenizer for an additional 1.5 hours at 20,000 rpm.

De-Gas: The homogenized SWCNTs/EG/phenolic resin mixture was poured into the prepared mold and heated to 65°C for 3-4 hours in vacuum. This allows the remaining EG and IPA from the resin to evaporate out and helps prevent voids within the sample. At this point a thin film of the composite material was spread onto a G-10 fiberglass beam of approximately 100 mm length by 8.3 mm width for the RLT test specimens.

Pre-Cure: The RLT coupon and composite mixture in the mold was heated to 120°C with an 18 hour ramp, at a rate of 5.5°C/hr. This slow ramp rate is necessary to achieve a sample that is free of voids. The sample/mold was removed from the oven immediately when 120°C is reached. The cured composite coupon was then allowed to cool in the mold with a weight on top to prevent bowing. After this cure cycle, the coupon was cut down to smaller pieces since it is not as stiff and brittle at this stage as it is after the final cure.

Final Cure: The composite coupons were prepared on a flat aluminum surface with an opposing aluminum plate placed on top of the coupons. The mass of the top plate provided approximately 0.05-0.10 lbs/in^2 of pressure on the coupons. If the mass is too large, there is a tendency to form cracks in the sample during final cure, whereas if the mass is too small the composite coupon will curl. The composite and RLT coupon was post-cured in a vacuum oven using a ramp rate of

1.5°C/min and held at 200°C for 1 hour. It was then cooled to ambient temperature under vacuum.

3.3 Characterization Techniques

3.3.1 CNT Characterization

Many techniques can be used to produce CNTs, but all processes create an inhomogeneous mixture of CNTs with varying degrees of metal catalyst and other carbon compounds, including amorphous carbon and fullerenes. Also, the CNT chirality, diameter, length, and surface chemistry can vary depending on the fabrication procedure. In addition to variations in the CNT production procedure, there are also several processes being used to purify the CNTs, which remove much of the contaminants but can also alter the length and surface chemistry of the nanotubes (Arepalli, et al., 2004). It is important to understand the characteristics of the nanotubes prior to fabrication of CNT composites, and/or to verify cleanliness of the CNTs prior to surface functionalization. For this research, the NASA-JSC protocol, authored by S. Arepalli et al (2004), was used as a guide for the characterization of the HiPco SWCNTs. The purified HiPco SWCNTs were characterized using Raman spectroscopy, thermogravimetric analysis (TGA), scanning electron microscopy (SEM) and energy dispersive spectroscopy (EDS), TEM, and ultra violet-visible (UV-VIS) spectrometry. The phenyl sulfonated SWCNTs were characterized using Raman spectroscopy and X-ray photoelectron spectroscopy (XPS).

3.3.1.1 Raman

Raman is commonly used in characterizing CNTs. The basis for Raman spectroscopy is in reflecting light off of a material and collecting the scattered light. Typically the photons will be scattered elastically, having the same energy and frequency as the incident light. However, a small percentage will be scattered inelastically, having emitted or absorbed a phonon, resulting in a change of frequency of the emitted light. Those photons having frequencies different from the incident light are used to produce the Raman spectra.

The Raman spectroscopy system used in this study is a Renishaw inVia. It works by directing a 785nm laser beam through a series of mirrors and a 20x microscope lens onto the sample. The emitted light is passed through a filter, which reflects back the elastically scattered photons and allows the inelastically scattered photons to pass through. The filtered light is then reflected off a diffraction grating, which separates the light according to its frequency and is then collected and analyzed by the Raman spectrometer. The Raman spectrum is produced, which plots the intensity versus the Raman shift.

The Raman spectrum displays a series of peaks, which can provide information about the nanotubes. Such peaks are known as the radial breathing mode (RBM), the D-band, and the G-band. The RBM is a set of peaks that fall in the 100 to 400 cm^{-1} range (Saito, Fantini, & Jiang, 2008) and is a unique characteristic of CNTs. The RBM arises from vibrations of the carbon atoms in the radial direction due to the focused laser beam. The RBM can be studied to determine nanotube chirality as well as the diameter or average diameters of the nanotubes

(Saito, Fantini, & Jiang, 2008) and whether the nanotubes are bundled (Arepalli, et al., 2004). In this study, the RBM is primarily used to confirm the existence of nanotubes. The D-band, located at approximately 1300 cm^{-1} range (Saito, Fantini, & Jiang, 2008), provides an indication of the disorder in the nanotubes. Imperfections such as defects, functionalization, and impurities will increase the intensity of the D-band. The G-band is made up of a double peak called the G^+ and G^- peaks. The G^+ peak is generally located near 1592 cm^{-1} (Saito, Fantini, & Jiang, 2008), and has the greatest intensity in the Raman spectra. The G^- peak is typically located near 1570 cm^{-1} (Saito, Fantini, & Jiang, 2008) with much lower intensity than the G^+ peak. The Raman spectra of graphite, which has similar structure to CNTs, displays a G-band that is only comprised of one peak relating to the excitation of the carbon bonds along the plane. However, due to the tubular nature of CNTs, the G-band forms two peaks, corresponding to the tangential (G^-) and axial (G^+) vibrations of the carbon bonds (Saito, Fantini, & Jiang, 2008). The G-band is also affected by mechanical strain imposed on the carbon bonds in the axial direction of the CNTs, giving rise to the Raman load transfer testing (see section 3.3.2.2). The ratio of G-band intensity (G^+ peak) to the D-band intensity can provide an indication of the purity of the nanotubes.

A total of three small samples were prepared on a glass slide and focused under the 20x magnifying lens. Raman spectra were obtained from each of the three samples using a 785nm laser.

3.3.1.2 TGA

TGA is a common technique for characterizing the thermal stability of CNTs. The principal behind TGA is in heating a material, usually in an oxidative atmosphere such as ambient air, and simultaneously measuring the weight. As the material oxidizes, the weight changes and the oxidation temperature can be determined by the derivative of the temperature vs. weight plot. Since residual metal catalyst in the SWCNTs can catalyze oxidation of CNTs at lower temperature, this can provide information regarding the presence of impurities in the SWCNT material.

TGA samples were prepared by placing 3mg of the purified SWCNT material into the alumina test apparatus crucible. The testing was performed using ambient air at a flow rate of 100 sccm and a heating rate of 5°C/min from ambient up to 850°C. Three samples of the material were tested, providing average peak oxidization temperature and standard deviation. Average oxidation temperature can provide information about the purity of the material while the standard deviation of the oxidation temperature provides an indication of the homogeneity of the material.

3.3.1.3 UV-VIS Near Infrared Spectroscopy

UV-VIS is a characterization technique used to analyze the dispersibility of the SWCNTs. The Perkin Elmer Lambda 900 UV-VIS near infrared spectrometer measures the optical density of the CNTs in solution. Impurities and large agglomerations of CNTs that are unstable in the solution will gradually fall out of suspension causing a reduction in the optical density of the solution. The change in optical density over time provides a measure of dispersibility. This can

be valuable in understanding the solubility of the CNT material in solvents and the ease of producing a well-dispersed CNT composite.

UV-VIS was used to determine the suspension stability of the SWCNTs in dimethyl formamide (DMF). Three samples were prepared by combining 0.1 mg of SWCNTs and 10 ml DMF in a sealed test tube and placing in a sonic bath for one hour. The dispersed solution was transferred to quartz cuvettes and immediately analyzed in the UV-VIS spectrometer to obtain the optical density of the solution. One hour later the optical density of the sample was measured again. The average dispersion stability was calculated by the percentage change in the area under the UV-VIS curve over one hour, from 700nm to 1000 nm. The average change of optical density provides an indication of the dispersion stability of the CNTs while the variation between samples of the optical density provides an indication of the homogeneity of the CNT material.

3.3.1.4 SEM and EDS

SEM is a common characterization technique that can provide a qualitative point of view on the amount of impurities that exist in the CNTs. SEM uses electrons, which interact with the atoms near the surface of the material and cause secondary scattering and backscattering. The secondary scattering of CNTs is detected by the SEM and the intensity is gathered point by point to produce an image of the material's surface. The source of the electron beam is usually a tungsten filament, lanthanum hexaboride (LaB_6) crystal, or field-emission gun (FEG). The size of the beam affects the resolution of the image and is usually between 3-5 nm.

A Hitachi S-4800 SEM was used to image the samples at 1.0 kV accelerating voltage. Samples were prepared by mounting a small amount of material on double sided carbon tape and coating with a thin layer of platinum to improve conductivity and prevent charging of the sample.

EDS detectors in the SEM pick up characteristic X-rays of the element being analyzed. These X-rays can be used to determine the composition of contaminants or impurities in the CNT sample.

3.3.1.5 TEM

TEM also provides a qualitative point of view on the amount of impurities that exist in the CNTs. It uses an electron beam, usually created by either a tungsten filament, lanthanum hexaboride (LaB_6) crystal, or FEG. The resolution obtained by TEM is better than that of SEM, and is on the order of about 0.3 nm, allowing better resolution on the nanotube scale. The TEM images were taken in bright field mode at a range of 150KX to 180KX in a JOEL high contrast TEM. In bright field mode, thicker sample sections or materials with higher atomic weights will show up darkest, allowing for speculation of whether observed impurities are amorphous carbon or metal catalyst. Like SEM, the TEM images are able to provide a subjective estimate of the sample purity.

3.3.1.6 XPS

XPS works by emitting a beam of X-rays at a material in a vacuum. The energy and number of scattered electrons is measured and analyzed to provide information regarding the elemental

compositions and electronic state present near the surface of the material. It is particularly useful in determining the degree of functionalization of surface modified CNTs.

XPS was performed using a PHI Quantera Microprobe system with monochromatic Al Kα (1486.6 eV). An aluminum anode was used at 15kV with a 200μm spot size and incidence angle of 90°. Three samples of phenyl sulfonated SWCNTs were prepared on indium foil, using beryllium copper clips to make electrical contact. Each of the three samples were survey scanned (full spectrum) and for some peaks, localized scans were obtained. Survey scans were acquired using a 140 eV pass energy, step size of 0.5 eV, and one sweep over the range of 0 to 1100 eV. Localized scans were accomplished using a 55 eV pass energy, step size of 0.2 eV and a 15 eV range centered at the peak of interest. The PHI data analysis software was used to compare the elements present in the material.

3.3.2 Composite Analyses

In this study, the composite material was evaluated using three techniques. Optical microscopy was used to analyze the level of dispersion attained during the homogenization process of the composite fabrication and SEM was performed to analyze the dispersion of CNTs within the cured composite. Dispersion within the matrix is widely believed to be the key to successful mechanical strengthening of the composite. Optical microscopy and SEM provide a means of subjectively evaluating whether the dispersion is reduced by increasing the SWCNT concentration. RLT was performed to determine the ability of the SWCNTs to bear load imposed

on the composite. The degree of load transfer to the SWCNTs from the matrix provides an indication of strengthening potential of the composite due to the integration of CNTs.

3.3.2.1 Optical Microscopy

Optical microscopy of the uncured SWCNT composite system can provide a subjective indication of dispersion of CNTs within the uncured composite after high shear mixing. The samples were prepared by placing a drop of homogenized SWCNTs/EG/Phenolic resin mixture on a glass slide. The mixture was then viewed under a Keyence VHX-100 digital microscope at magnifications up to 1000x. Light was transmitted through the sample for imaging.

3.3.2.2 Raman Load Transfer

The Raman spectra display a series of peaks, which can provide information about the CNTs. One of those peaks is the G^+ peak that corresponds to axial vibrations of the carbon bonds. The G^+ peak is affected by strain imposed on the carbon bonds in the axial direction of the CNTs, allowing measure of load transfer in a CNT composite material. If strain imposed on a composite matrix is transferred to the SWCNTs, a shift in the G-band will be observed in the Raman spectra and can provide a relative comparison of load transfer.

A Renishaw inVia was used to obtain Raman spectra of the material. One test coupon was prepared for each concentration of SWCNT/phenolic resin composite. The test specimens were prepared by applying a thin film of the composite mixture onto a fiberglass beam of dimensions

100mm length, 8.3mm width, and 2.35mm thickness. The thin film was subsequently cured per section 3.2. In all RLT test specimens, the SWCNTs were randomly within the thin film.

A four point bend apparatus was set up and strain gauge applied to a dummy fiberglass beam of same thickness as those used for the test specimens. Both the strain gauged beam and the test specimen were loaded into the four point bend apparatus and measurements were taken at 10 locations on the test specimen near the strain gauge. Since the thickness of the composite film on the test specimen beam is approximately 20 μm, the strain through the composite is assumed to be nearly the same as that of the strain gauge and throughout the thickness of the thin film. The four point bend apparatus was set up in tensile configuration and measurements were taken in the same 10 locations from zero strain up to 0.8% strain at an increment of 0.2%. The four point bend apparatus was then switched into compression configuration and measurements were taken in the same 10 locations from zero strain to -0.8% strain at an increment of 0.2%. A schematic of Raman load transfer apparatus is presented in Figure 1. A partial hysteresis loop was acquired for the Raman shift vs. strain. The plot was normalized for the purpose of evaluation (i.e. the relative Raman shift was set to zero for Raman measurements under zero strain). This normalized plot allows calculation of the average slope and total change of Raman shift for the test specimens of each SWCNT concentration. Larger slope and change of Raman shift indicate that a greater amount of the load is transferred to the nanotubes.

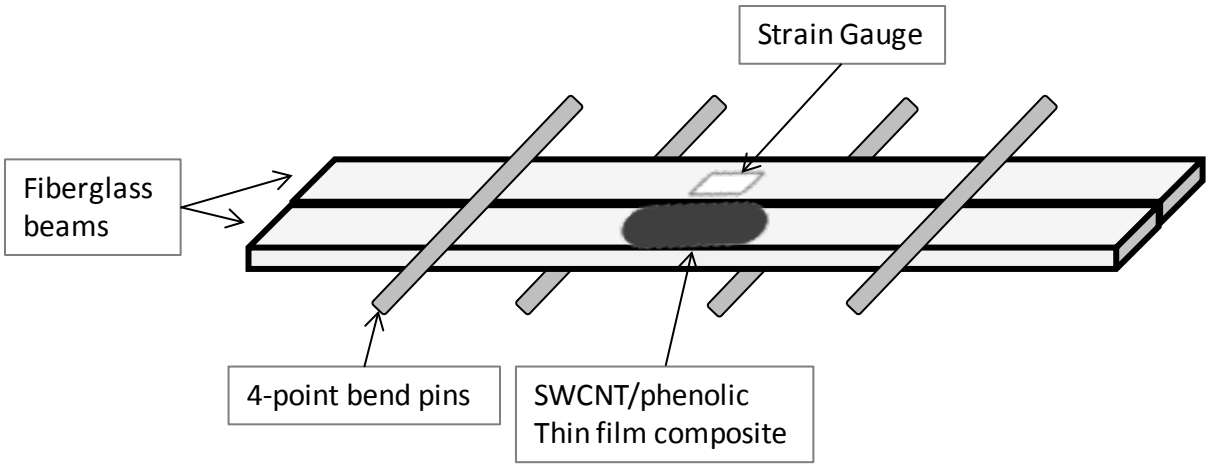

Figure 1: A schematic of Raman load transfer test apparatus.

3.3.2.3 SEM of Composite

SEM examination of a SWCNT composite can provide a subjective indication of nanotube pull-out and dispersion in the matrix. A Hitachi S-4800 SEM was used at 1.0 kV accelerating voltage. The samples were prepared by mounting a fractured sample of composite material on double-sided carbon tape and coating with a thin layer of platinum to prevent charging.

4 RESULTS AND DISCUSSION

4.1 Characterization of Purified SWCNTs

Purified HiPco SWCNT material was characterized using Raman spectroscopy, TGA, SEM and EDS, TEM, and UV-VIS spectrometry.

4.1.1 Raman

Figure 2 presents Raman spectra of the D- and G-bands from each sample of purified HiPco with the RBM spectra as an inset. The line shape of the RBM spectra is very similar to previous measurements of purified HiPco material (Arepalli, et al., 2004), (Chiang, et al., 2001) and lies within the range of approximately 200 to 300 cm^{-1}. Typically RBMs lying between 120 and 350 cm^{-1} indicate that the SWCNTs have a diameter within the range of .7 to 2 nm (Dresselhaus, Dresselhaus, Saito, & Jorio, 2005). This is expected for HiPco SWCNTs, which generally have an average diameter of approximately 1.1 nm (Chiang, et al., 2001).

In the Raman spectra, the region from 1330 to 1500 cm^{-1} does not exhibit any strong peaks. Peaks in that range are characteristic of amorphous carbon. This suggests that most of the amorphous carbon was removed from the SWCNT material during the purification process.

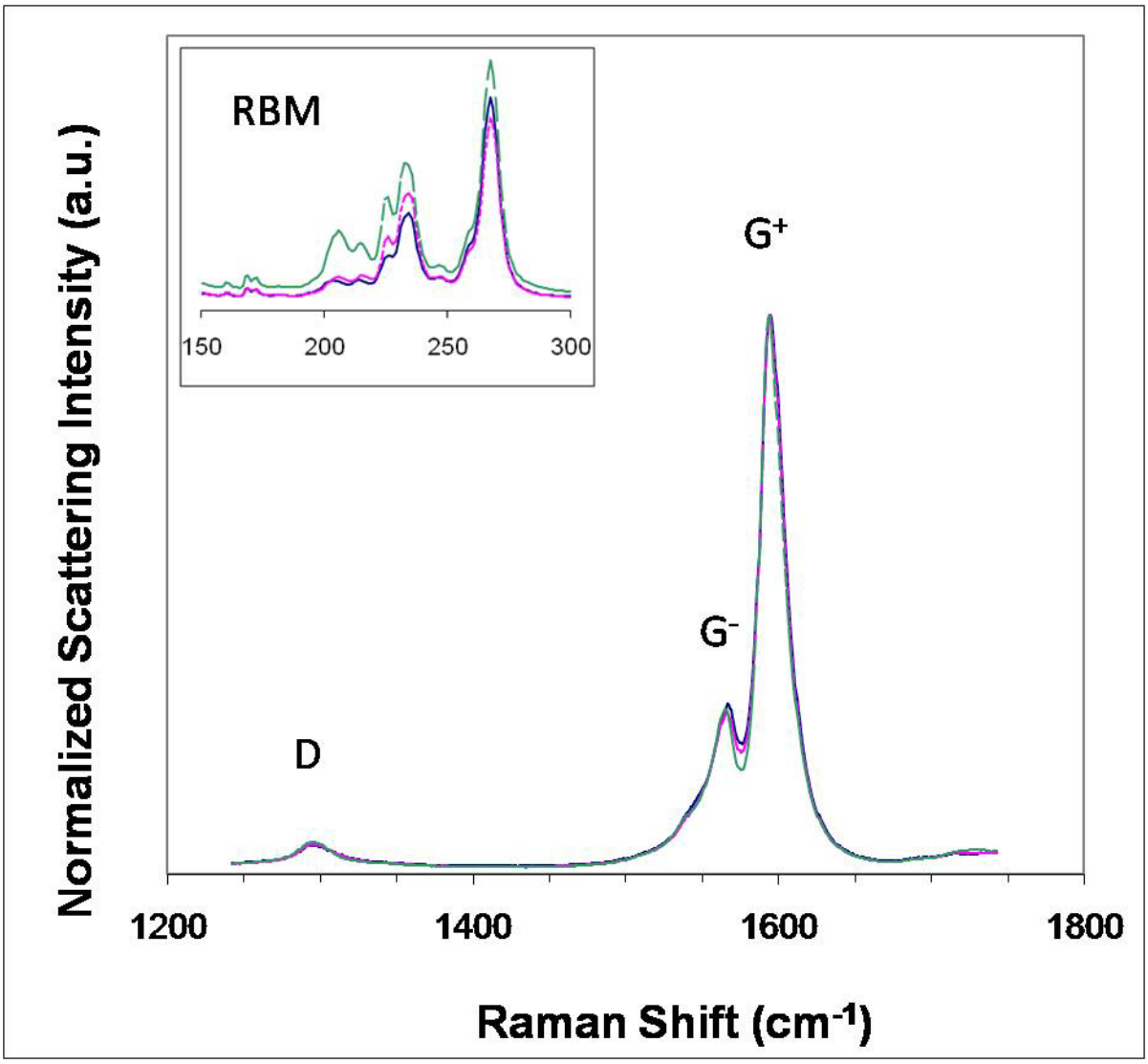

Figure 2: Raman spectra of purified HiPco SWCNTs localized at the G-band region. RBM region is in the inset.

The D-band is located at a Raman shift of 1295 cm^{-1} with a width (at half max) of approximately 30 cm^{-1} as shown in Figure 2. According to Arepalli, et al. (2004), a D-band that is shifted further to the right and/or has a larger width corresponds to the presence of graphite and/or

amorphous carbon. The D-band observed for SWCNTs employed in this study suggests that very little graphite and amorphous carbon exist in the SWCNTs.

The ratio of intensity of the D- and G-bands, as labeled in Figure 2, provides an indication of the disorder in the SWCNTs, which can arise from impurities as well as surface modifications. The average D/G ratio of three samples of purified SWCNTs is 0.054 with a standard deviation of 0.0028. The low D/G ratio is similar to previous results (Arepalli, et al., 2004) and suggests that most impurities have been removed from the HiPco SWCNTs. The low standard deviation suggests good homogeneity within the three samples that were analyzed.

The G-band, shown in Figure 2, exhibits Lorentzian lineshape, which means that the SWCNTs are semi-conducting rather than metallic (Dresselhaus, Dresselhaus, Saito, & Jorio, 2005). This is also to be expected for HiPco SWCNTs (Nikolaev, 2004). The average G-band position of the three samples is 1594.34 cm^{-1} with a standard deviation of 0.497 cm^{-1}. The G-band location is similar to previous measurements and the low standard deviation suggests good homogeneity within the three samples that were analyzed.

Overall, the Raman spectra indicate that the material is consistent with previously purified HiPco SWCNT material using the soft-bake procedure. The material has a low content of amorphous carbon and other impurities, and appears to have been properly purified.

4.1.2 TGA

The thermal stability of the purified SWCNTs was determined by performing TGA. Figure 3 shows a plot of the sample's weight (w) vs. temperature (T) and dw/dT for each of the three samples. CNTs generally oxidize into CO(g) or CO_2(g), causing a decrease in the weight as the temperature is increased. The plot of dw/dT shows the peak oxidation temperature for each sample, which is taken to be the temperature at the maxima. The average peak oxidation temperature of the three samples is 551.2°C with a standard deviation of 26.3°C. The mean oxidation temperature of this batch is similar to previous TGA results of purified HiPco SWCNTs (P.G. Moloney, personal communication, May 2008) and is relatively high compared to the typical value of 405.87°C, expected for HiPco SWCNTs before purification (Arepalli, et al., 2004). Lower oxidation temperature corresponds to the presence of metal impurities in the sample, which catalyze the oxidation reaction. The peak oxidation temperature for purified SWCNTs has been reported as high as 602°C (Arepalli, et al., 2004). The lower oxidation temperature observed could also be caused by a smaller average diameter or defects of the nanotube surface; however, the cause cannot be distinguished by TGA (Arepalli, et al., 2004). The oxidation temperature observed at 551°C still suggests that most impurities such as metals and amorphous carbon have been removed by purification. The oxidation temperatures of the three samples deviated significantly from their mean, which implies there is an inhomogeneity within the batch. However, the SWCNT material will undergo homogenization at least one additional time during composite fabrication and/or functionalization. TGA analysis suggests that the SWCNTs have been properly purified.

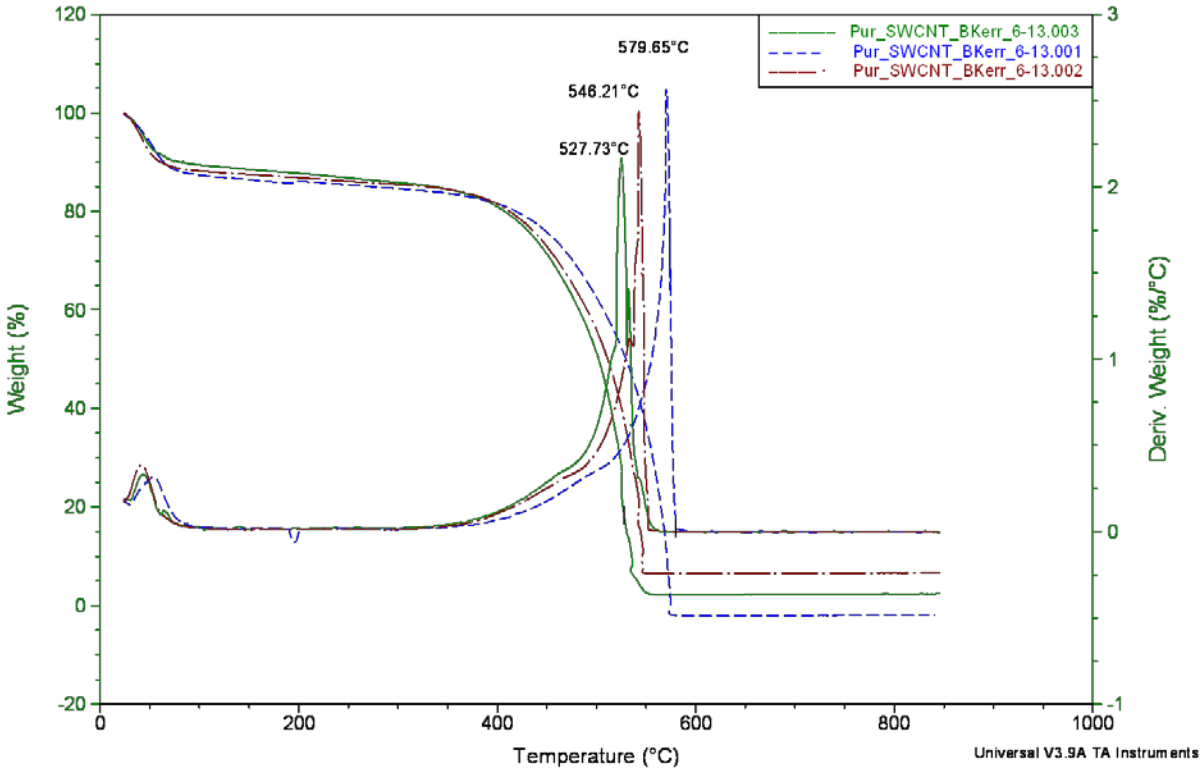

Figure 3: Weight change as a function of temperature, and its derivative (dw/dT), for three different samples of purified HiPco SWCNTs.

4.1.3 UV-VIS

UV-VIS was used to determine the suspension stability of the SWCNTs in DMF. The SWCNTs appeared dispersed in the DMF within about 15 minutes of sonication, about what is expected of purified SWCNTs according to the NASA-JSC protocol (Arepalli, et al., 2004). The change in optical density for samples 1, 2, and 3, presented in Figure 4 through Figure 6, was 2.54%,

8.75%, and 8.97%, respectively. The average decrease in optical density of the three samples was 6.75%, which means that the SWCNTs remained well suspended in the solution after 1 hour. The suspension stability appears consistent with previous data and is much higher than expected for raw material. The NASA-JSC protocol (Arepalli, et al., 2004) achieved a 2.95% decrease for purified nanotubes and a 65.9% decrease for raw material. There is a noticeable difference between the samples, with a standard deviation of 3.65%, which is likely due to inhomogeneity within the material.

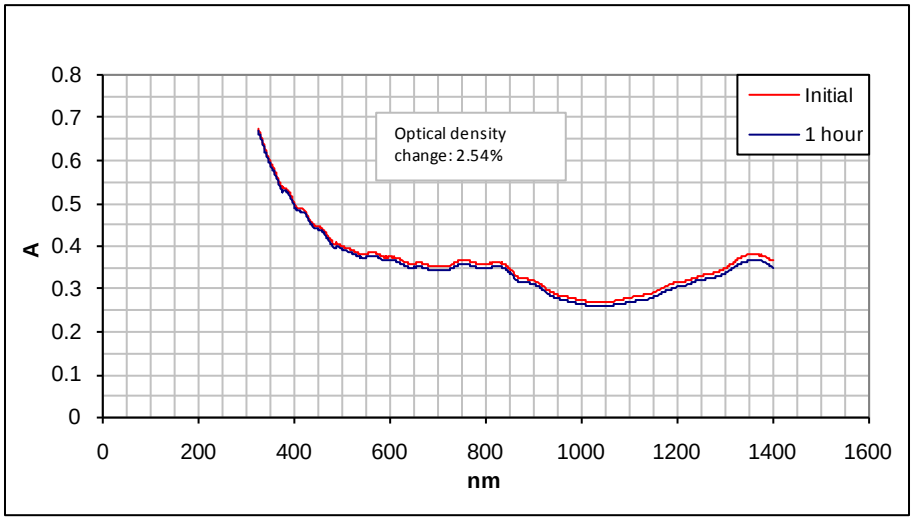

Figure 4: UV-VIS spectrum of purified SWCNTs (sample 1) suspended in DMF, immediately after sonication and 1 hour after sonication.

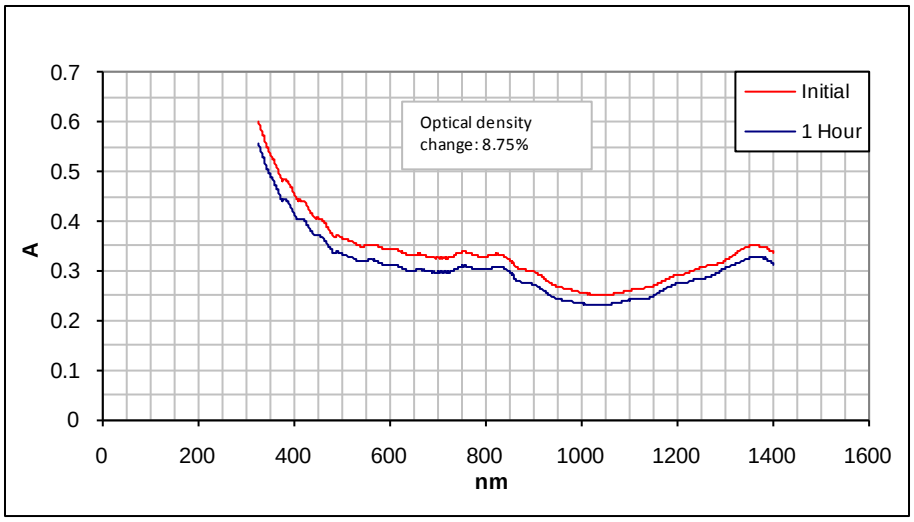

Figure 5: UV-VIS spectrum of purified SWCNTs (sample 2) suspended in DMF, immediately after sonication and 1 hour after sonication.

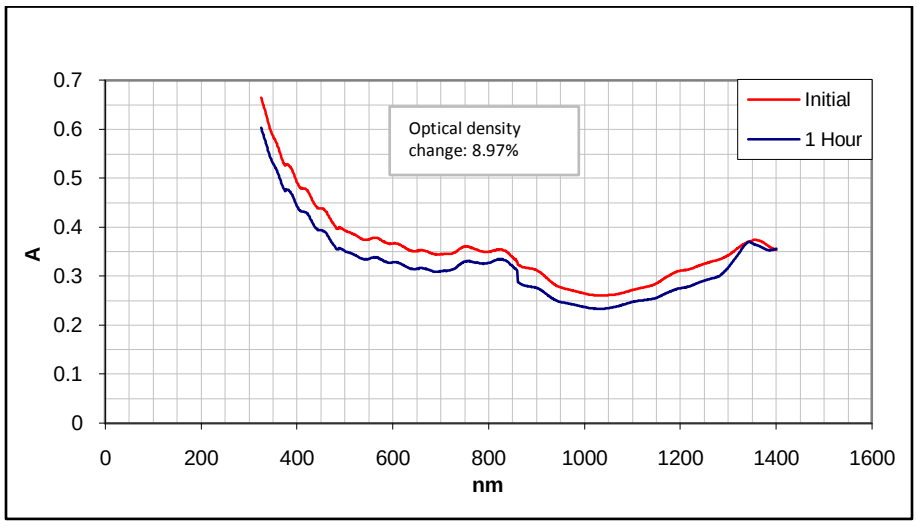

Figure 6: UV-VIS spectrum of purified SWCNTs (sample 3) suspended in DMF, immediately after sonication and 1 hour after sonication.

4.1.4 SEM and EDS

SEM can provide information on the presence of amorphous carbon and metal catalyst in the purified SWCNTs based on morphological differences. In general, the secondary electron micrographs show a relatively clean sample with a small amount of amorphous carbon and metal catalyst. Figure 7 shows some impurities among the SWCNTs that are likely either amorphous carbon or metal catalyst. Figure 8 and Figure 9 show clean nanotube bundles. In examining the purified SWCNTs using SEM, impurities appeared in groups at localized regions.

EDS from an area of material, approximately 500 μm^2 in size, indicated a strong presence of carbon and a weak presence of chlorine as shown in Figure 10. The chlorine is typically observed by EDS from soft-baked purified SWCNTs because of HCl used during the purification process. EDS was also performed on an impurity. The impurity, as presented in Figure 11, showed a strong carbon peak, likely correlating to amorphous carbon. Overall the SEM analysis demonstrated that the purified SWCNTs were clean with a small concentration of impurities.

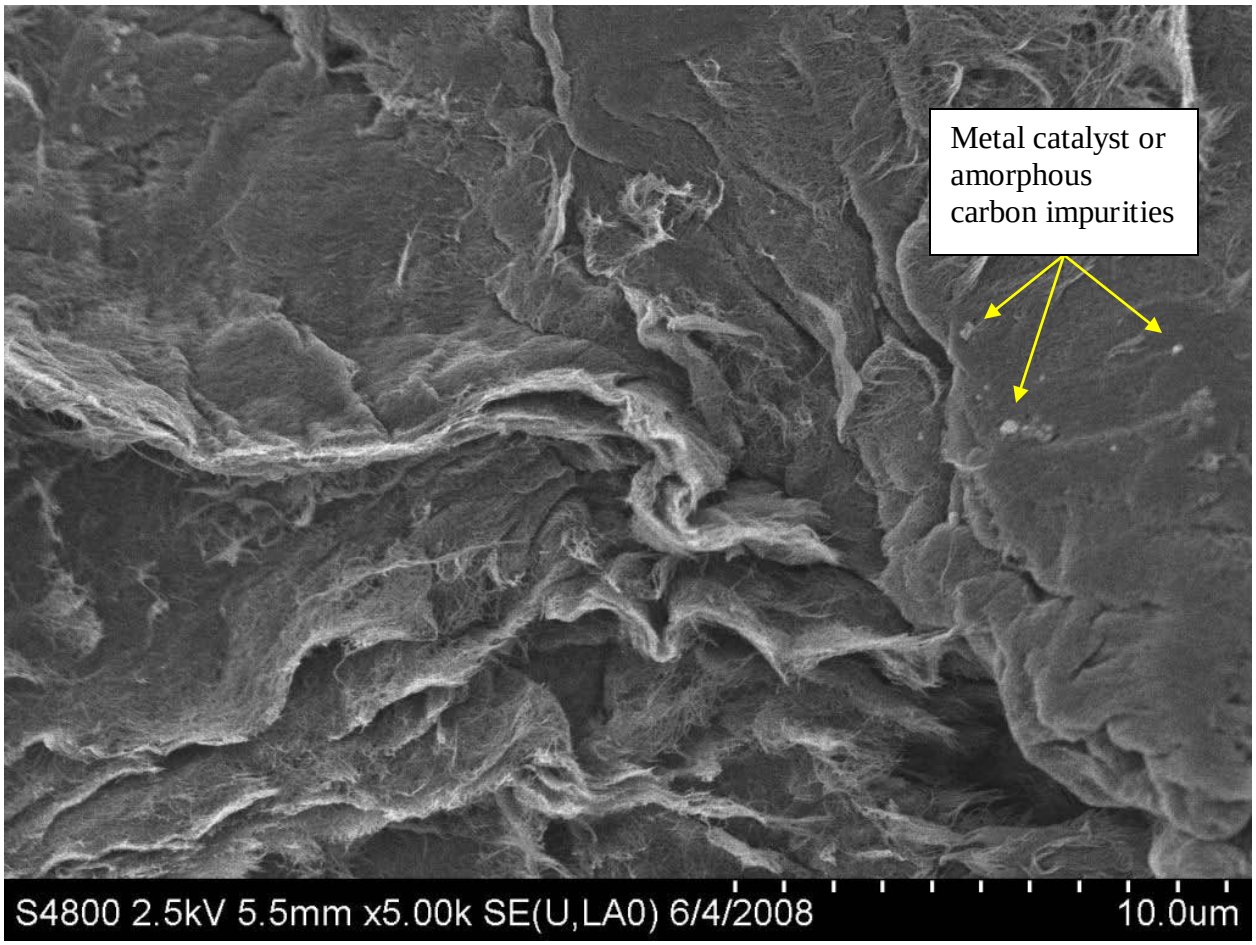

Figure 7: Secondary electron micrograph of purified SWCNTs.

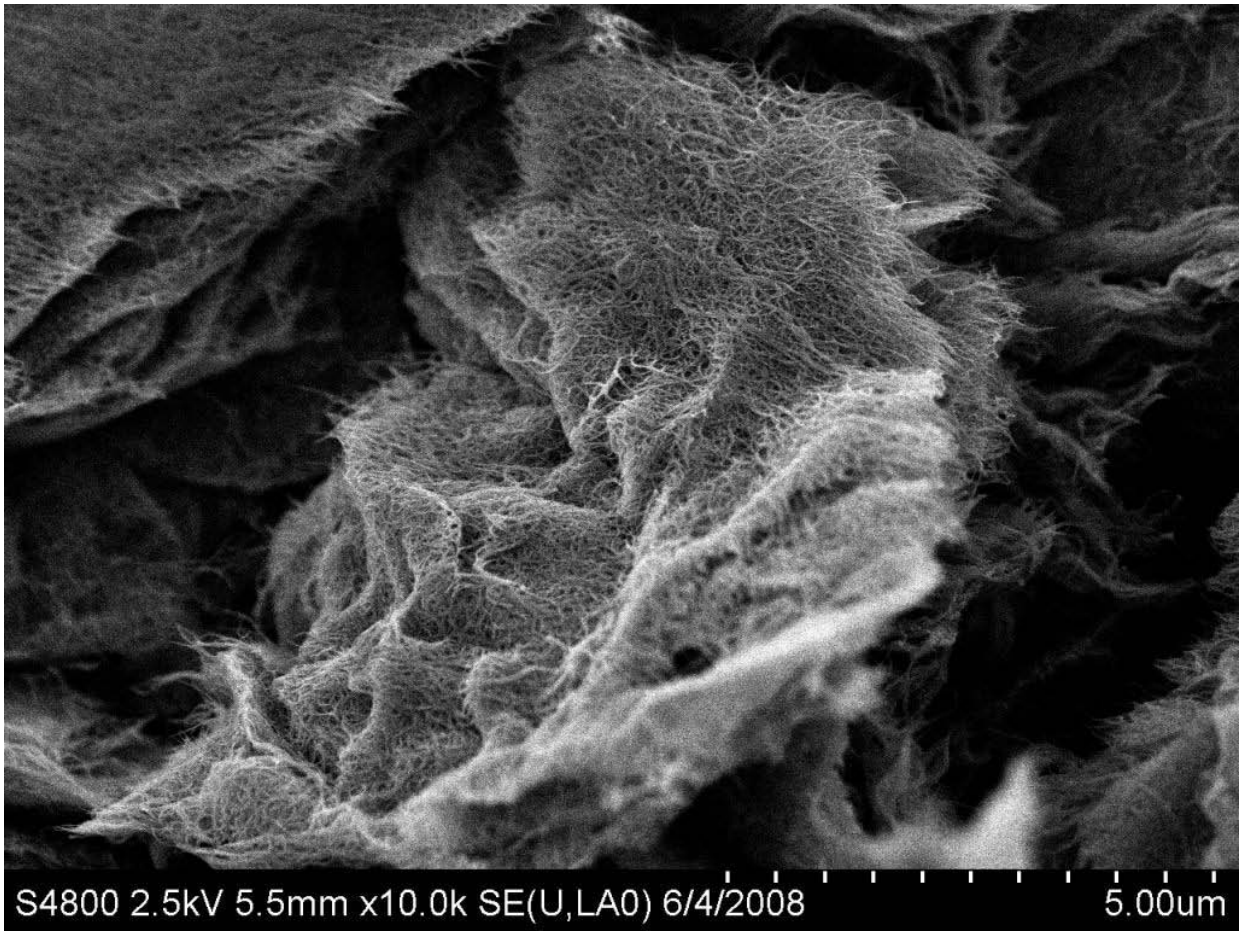

Figure 8: Secondary electron micrograph of purified SWCNTs at higher magnification.

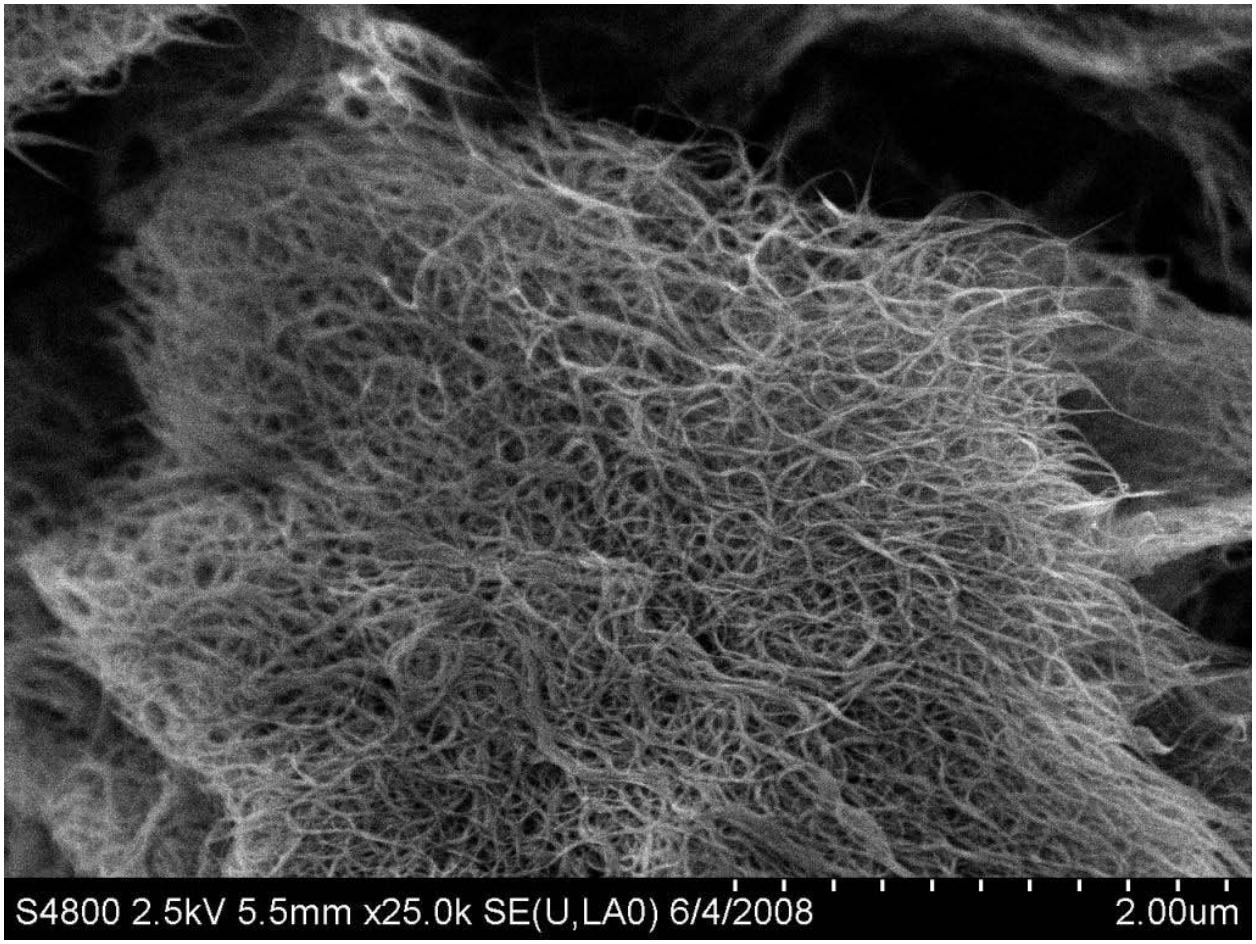

Figure 9: High resolution secondary electron micrograph of purified SWCNT bundles.

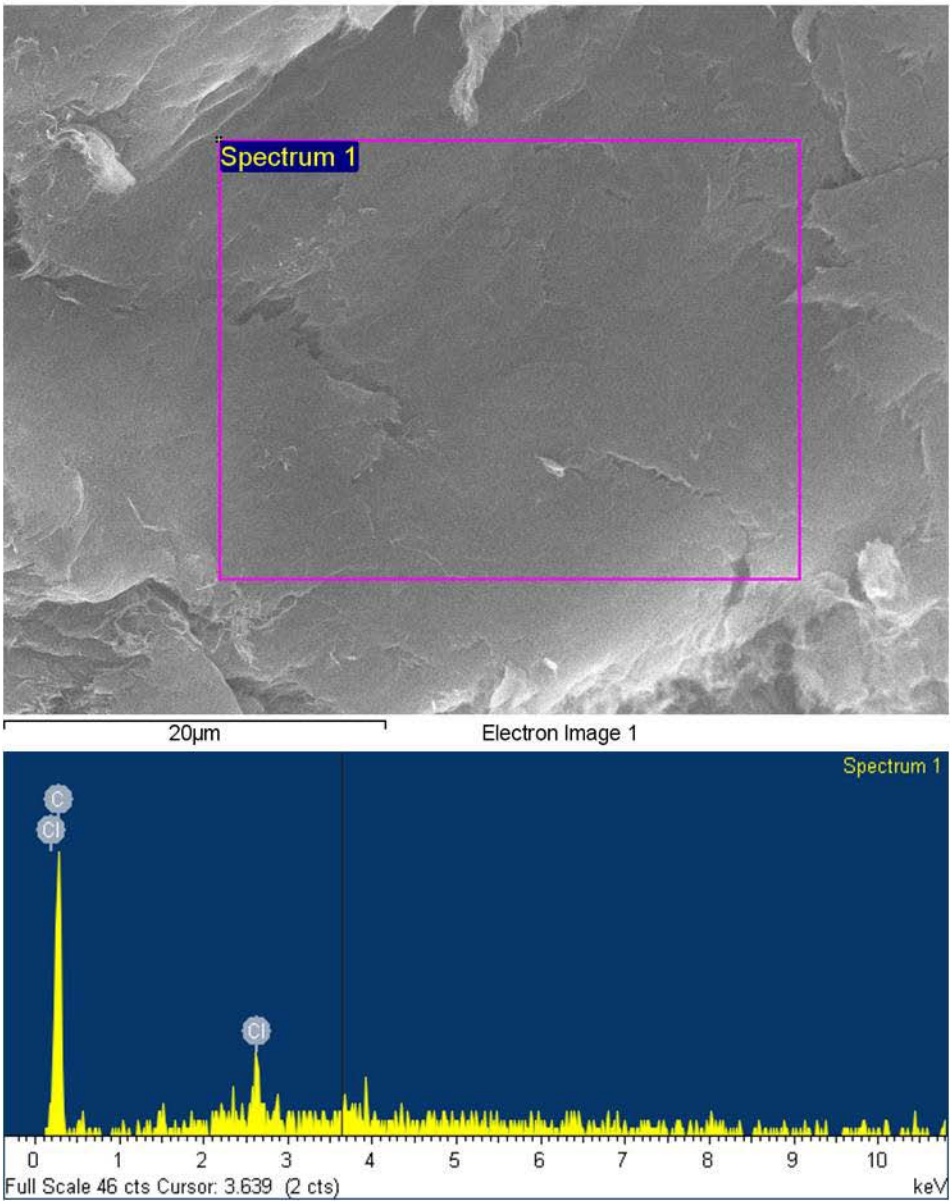

Figure 10: Secondary electron micrograph of purified SWCNTs and the corresponding XEDS spectrum showing carbon and chlorine peaks.

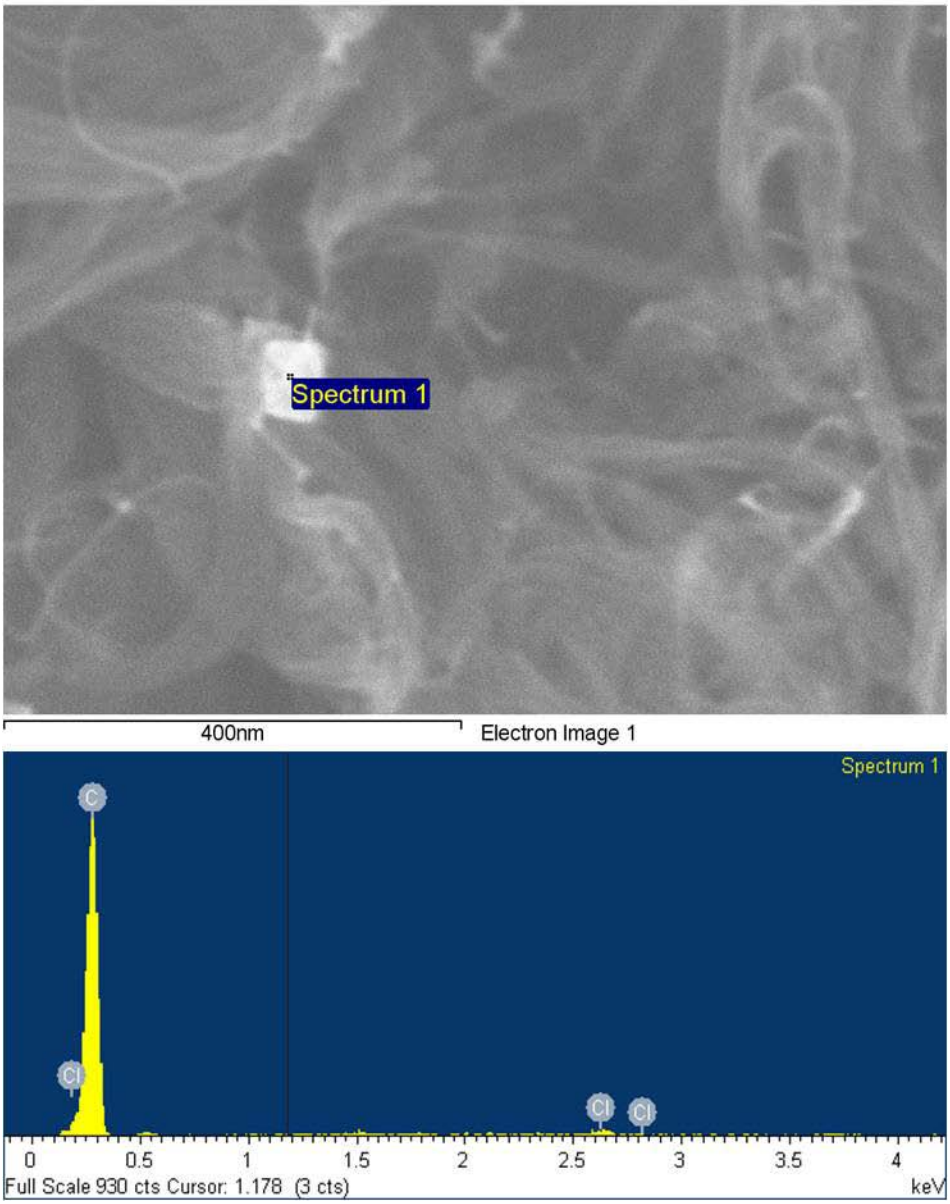

Figure 11: Secondary electron micrograph of purified SWCNTs and the XEDS spectrum obtained from location indicated where carbon and chlorine were observed.

4.1.5 TEM

Figure 12 presents bright-field TEM micrographs of soft-bake purified SWCNTs. These micrographs showed that a small amount of impurities exist in the material, on the order of what has been previously observed of soft-bake purified HiPco SWCNTs (P.G. Moloney, personal communication, May 2008). In particular, Figure 12(b) shows a nanotube bundle with a few dark spots, which are likely to be residual metal catalyst. As a comparison, Figure 13 shows bright-field TEM micrographs of the HiPco SWCNTs prior to the soft-bake purification procedure. These figures clearly demonstrate that the soft-bake purification procedure removed most of the impurities.

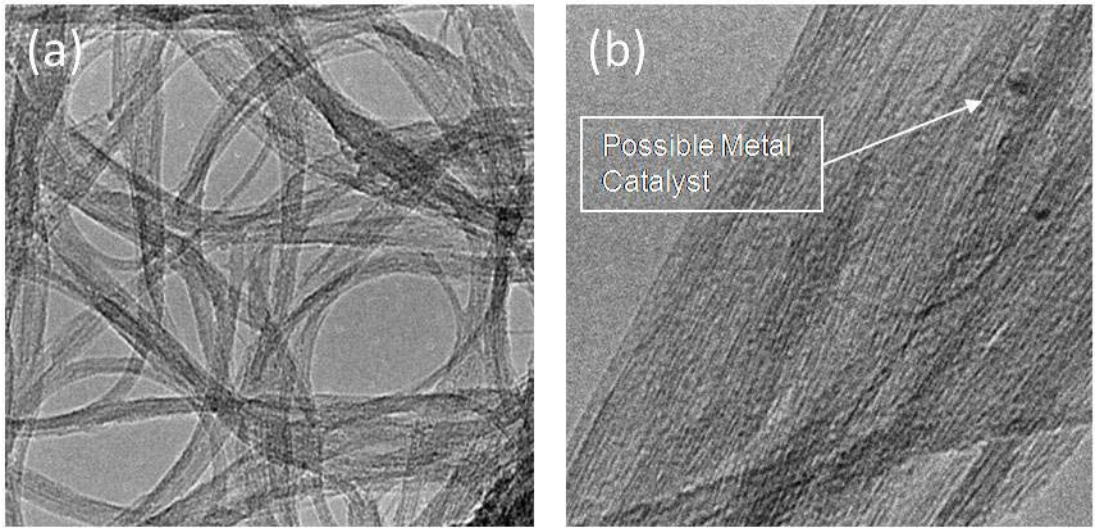

Figure 12: Bright-field TEM micrograph of soft-bake purified SWCNTs: (a) at 150kx, and (b) at 180kx magnification (Images Provided by Padraig Moloney)

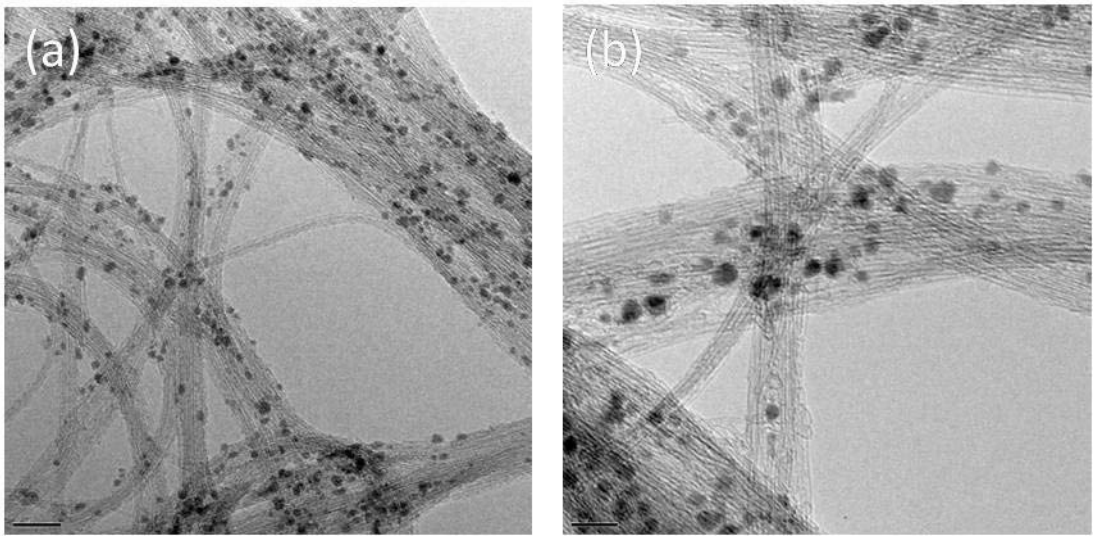

Figure 13: Bright-field TEM micrograph of HiPco SWCNTs prior to purification at two different locations: (a) at 150kx, and (b) at 180kx magnification.

4.1.6 Summary of Purified SWCNT Characterization

The purified HiPco SWCNT material was characterized using Raman spectroscopy, TGA, SEM and EDS, TEM, and UV-VIS spectrometry. Overall, the results suggest that this material was sufficiently purified to proceed with fabrication of a composite, and functionalization of the SWCNTs, followed by composite fabrication using functionalized SWCNTs. Although TGA, UV-VIS, and SEM results indicated that some inhomogeneity within the material exists, the material will undergo homogenization at least one additional time during either the composite fabrication process or the functionalization process. All other characterization results demonstrated that SWCNTs were sufficiently purified.

4.2 Analysis of Purified SWCNT/Phenolic Resin Composite

Composite test coupons were fabricated using purified HiPco SWCNTs. Four composite test coupons and four thin film composite RLT coupons were fabricated as described in section 3.2 at concentrations of 0.25 wt%, 0.50 wt%, 1.00 wt%, and 2.00 wt%. The composites were characterized using optical microscopy during fabrication, SEM for the fracture surface of the cured composite, and RLT of the thin film composite.

4.2.1 Optical Microscopy

Optical microscopy was carried out during the fabrication of each SWCNT composite. Figure 14 shows the dispersion of the 0.25 wt% SWCNTs in ethylene glycol and uncured phenolic resin at 100x and 500x magnifications. The dark gray areas correspond to dispersed SWCNT bundles. The black spots represent tightly bound clusters of SWCNT bundles, which likely will not be infiltrated with phenolic resin, and will not help to improve the strength of the composite. There are very few clusters in the 0.25 wt% sample, as shown in Figure 14, that are greater than 25 µm in diameter. Figure 15 shows the optical micrograph from the 0.50 wt% SWCNT composite and looks fairly similar to the 0.25% micrograph, shown in Figure 14. There appears to be a slight increase in the number of clusters that are greater than 25 µm in diameter. Figure 16 shows the optical micrograph for the 1.00 wt% SWCNT composite. In this image small air bubbles can be seen and appear as white circles with a black outline. There is a noticeable increase in size and number of undispersed SWCNT clusters, with many that are larger than 100 µm diameter. Figure

17 shows the optical micrograph for the 2.00 wt% SWCNT composite. This micrograph shows an even greater number of tightly bound clusters. They also appear larger than the others with some of the clusters as large as 200 µm in diameter. This is consistent with findings of Ryan, et al. (2007) and Yeh, Tai, & Liu (2006), who reported that the degree of dispersion of SWCNTs decreases as the concentration of nanotubes increases. Optical micrographs, Figure 14 through Figure 17, from the composites confirm this trend.

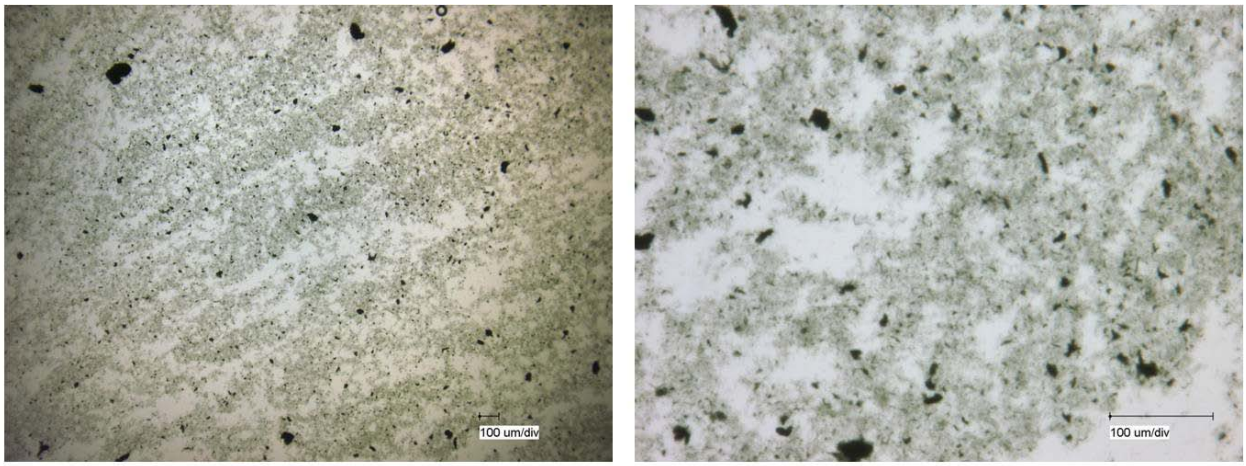

Figure 14: Optical micrographs of 0.25 wt% purified SWCNTs dispersed in ethylene glycol and uncured phenolic resin at: (a) 100x and (b) 500x magnification.

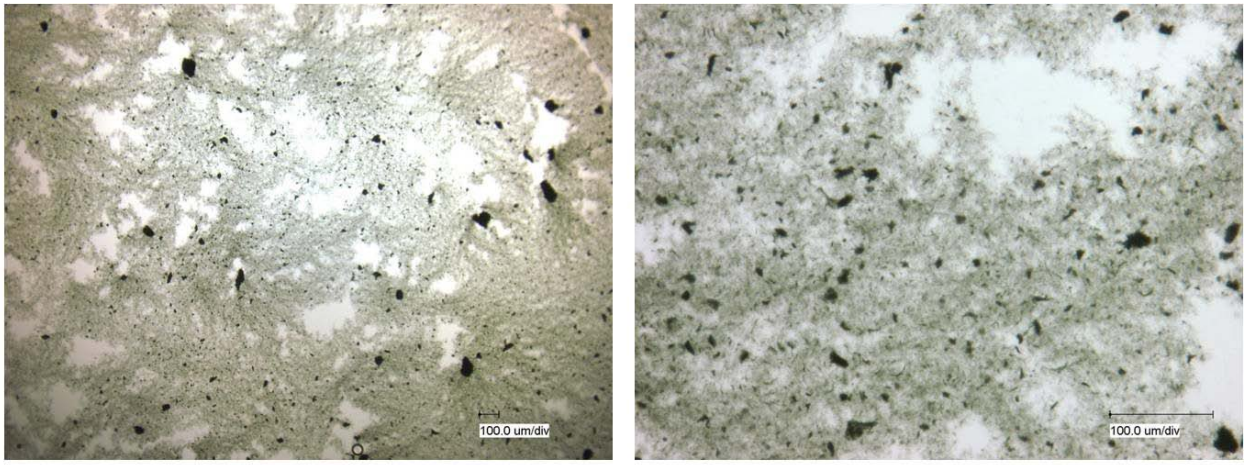

(a) (b)

Figure 15: Optical micrographs of 0.50 wt% purified SWCNTs dispersed in ethylene glycol and uncured phenolic resin at: (a) 100x and (b) 500x magnification.

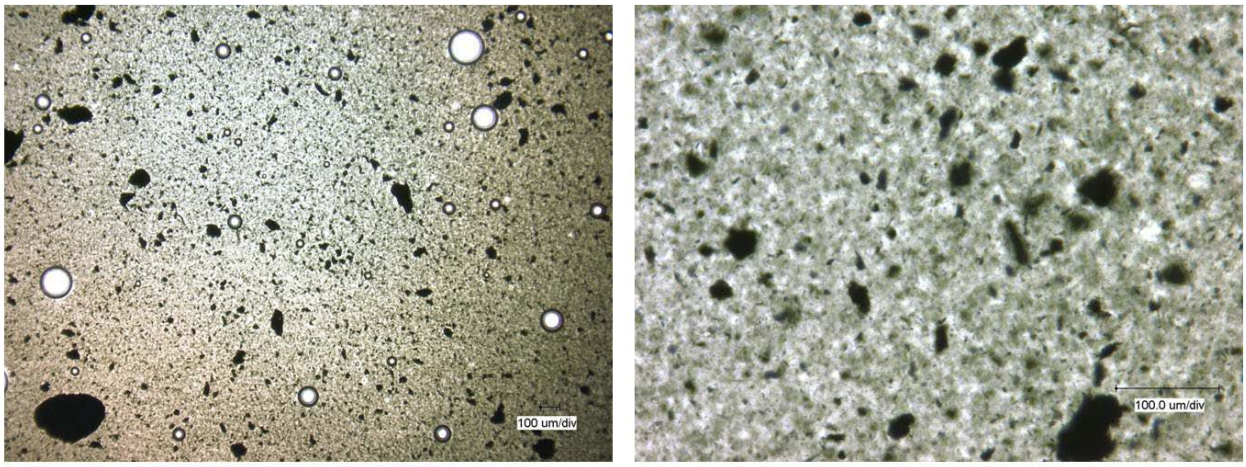

(a) (b)

Figure 16: Optical micrographs of 1.00 wt% purified SWCNTs dispersed in ethylene glycol and uncured phenolic resin at: (a) 100x and (b) 500x magnification.

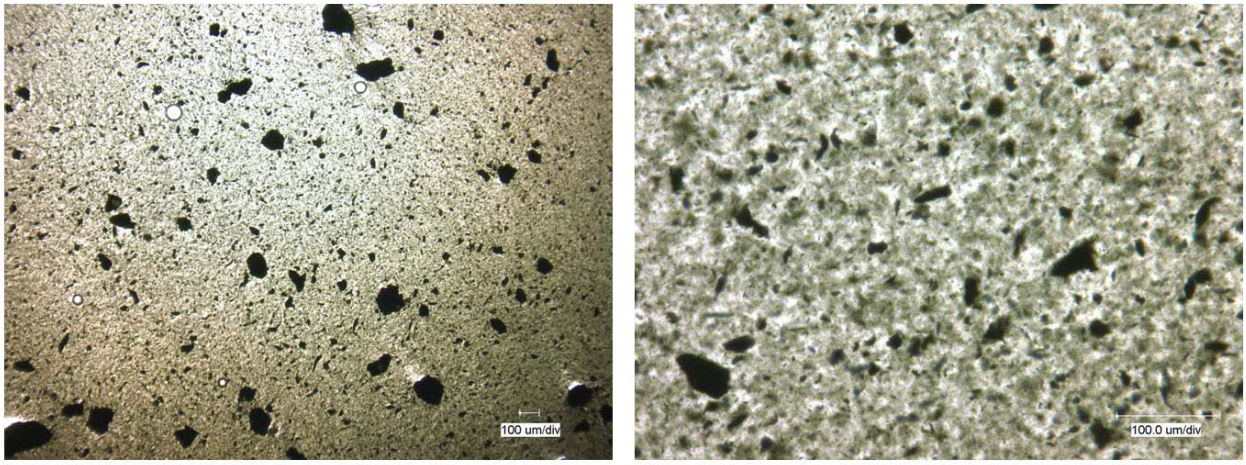

Figure 17: Optical micrographs of 2.00 wt% purified SWCNTs dispersed in ethylene glycol and uncured phenolic resin at: (a) 100x and (b) 500x magnification.

4.2.2 SEM

Figure 18 through Figure 21 show secondary electron micrographs from fractured composites with 0.25%, 0.50%, 1.00%, and 2.00% by weight of SWCNTs, respectively. These figures show nanotubes protruding from the fracture surface of phenolic resin matrix. It is likely that these are nanotube bundles that are protruding rather than individual SWCNTs as the diameters observed are much greater than that of individual nanotubes. The diameters appear to be on the order of 200 to 500nm. Individual nanotubes may not have been dispersed from bundles or they may have been masked by the deposited platinum, allowing us only to see bundles. Figure 18 (b) shows nanotube bundles that have been pulled out of the matrix. The nanotube pullout suggests that the strength at the nanotube/phenolic interface is weaker than the strength of the nanotubes. Figure 19 shows some areas where agglomerations have formed and nanotube bundles are bridging

across cracks in the matrix. This demonstrates that SWCNT bundles have absorbed some load from the composite. Figure 21 shows an area where the composite was fractured through the center of a cluster approximately 50 µm by 100 µm in size. It appears from this SEM image that the phenolic resin was not able to infiltrate the cluster. In Figure 21 (b) it can be seen that the perimeter nanotube bundles are partially embedded in the phenolic resin and are being stretched across a gap creating a bridging affect.

Based on SEM of fractured surfaces, as presented in Figure 18 through Figure 21, it appeared that the dispersion of SWCNT bundles was better at lower concentrations. This also correlates with the results of the optical imagery.

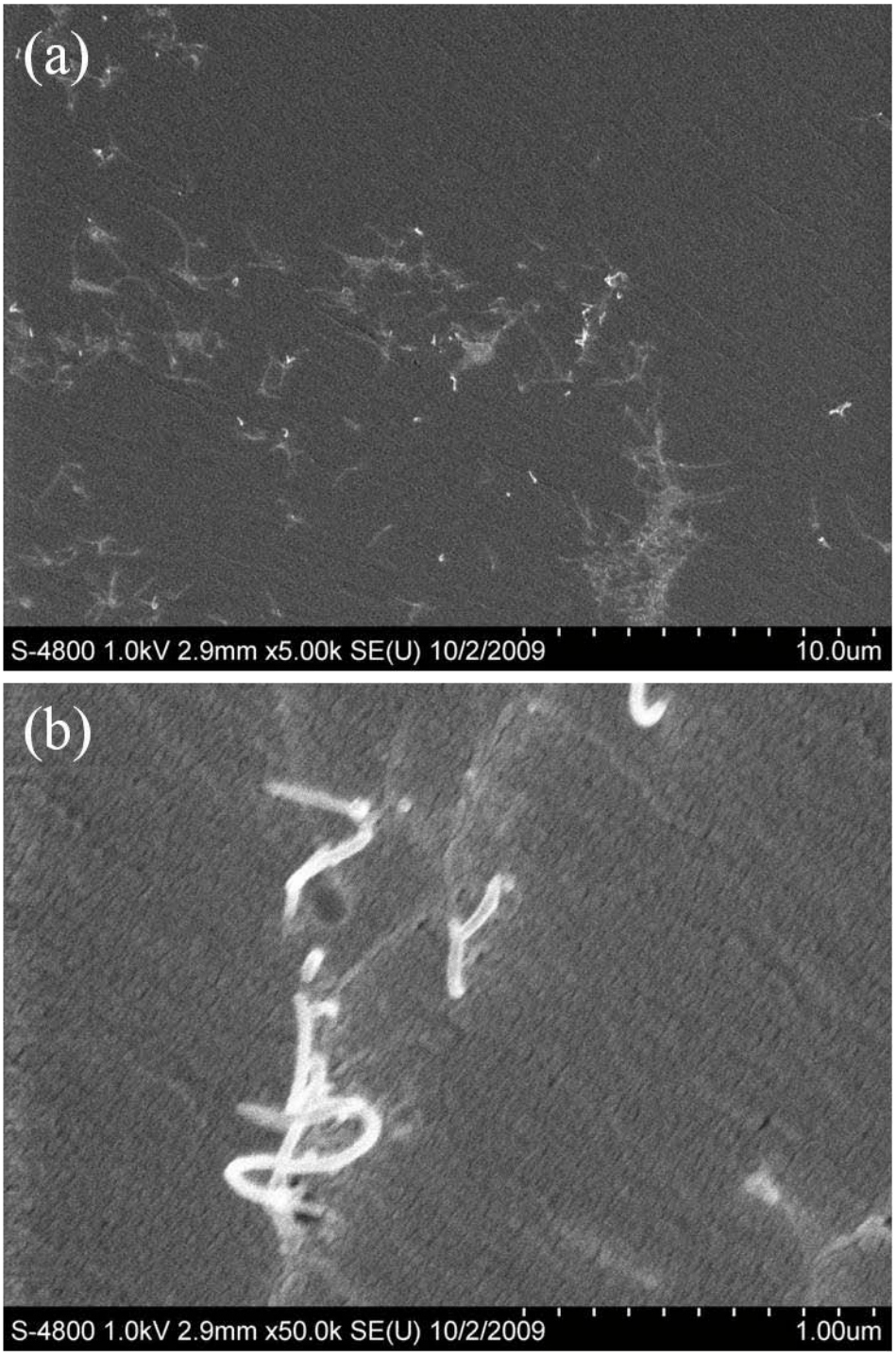

Figure 18: Secondary electron micrographs of 0.25 wt% SWCNT composite at: (a) 5kx and (b) 50kx magnification.

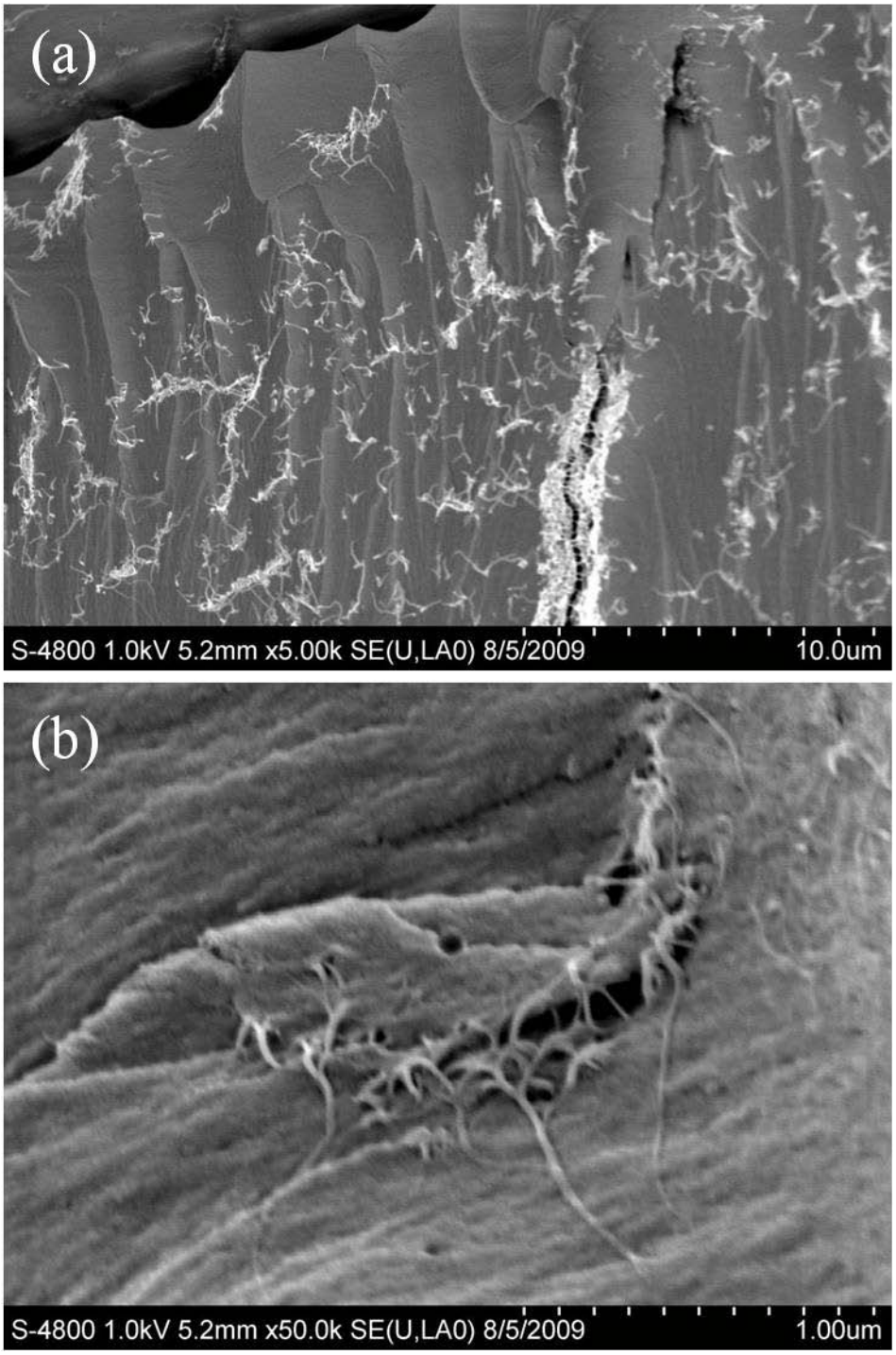

Figure 19: Secondary electron micrographs of 0.50 wt% SWCNT composite at: (a) 5kx and (b) 50kx magnification.

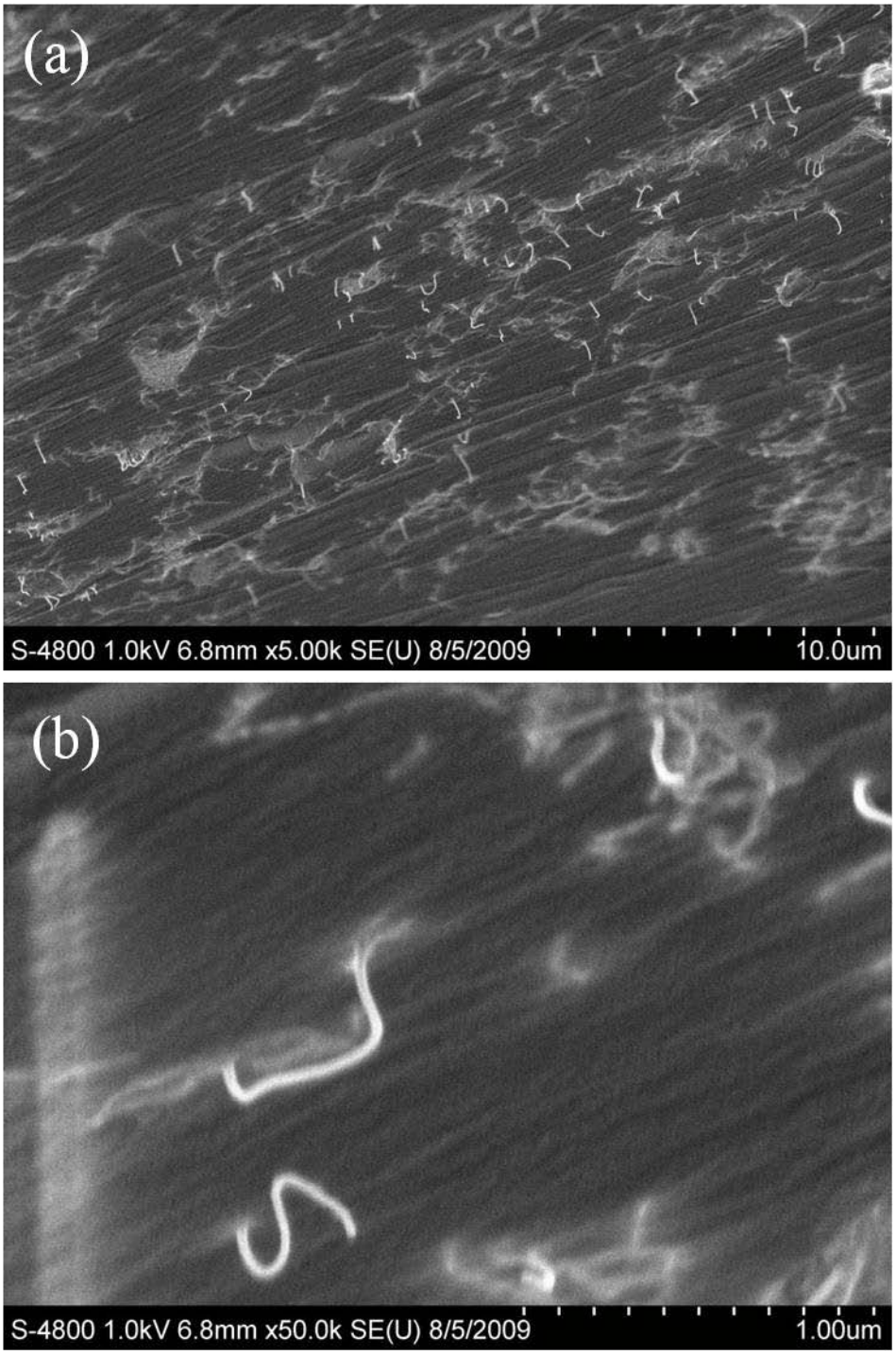

Figure 20: Secondary electron micrographs of 1.00 wt% SWCNT composite at: (a) 5kx and (b) 50kx magnification.

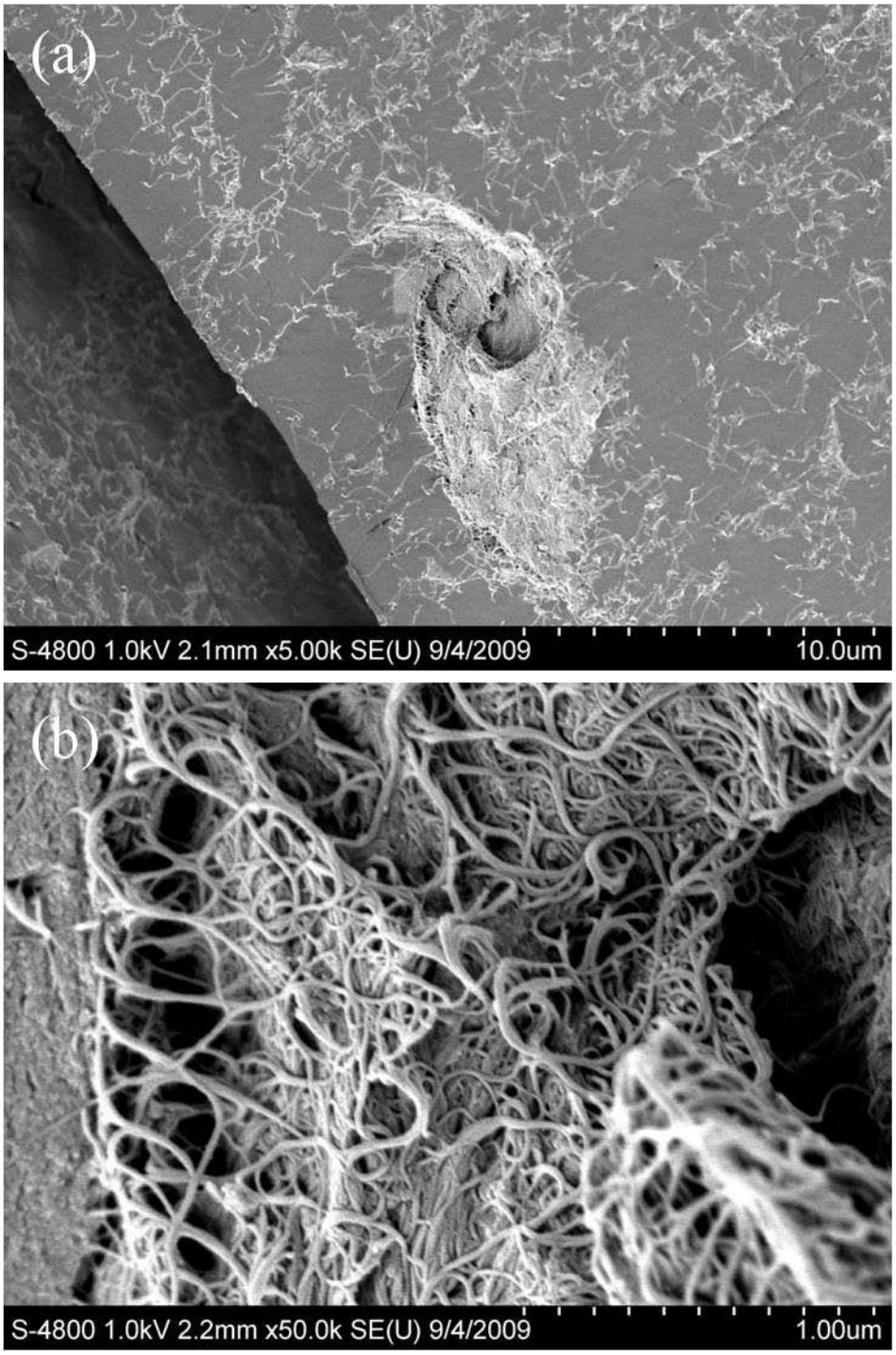

Figure 21: Secondary electron micrographs of 2.00 wt% SWCNT composite at: (a) 5kx and (b) 50kx magnification.

4.2.3 Raman Load Transfer

Figure 22 shows an example of the down-shift of the G-band due to tensile strain. The average G^+ peak position is graphed as a function of strain in Figure 23 for the composites with varying SWCNT concentration. A solid line drawn in Figure 23 represents the G-band shift as a function of strain when there is 100% load transfer from the matrix, as calculated from findings by Cronin et al. (2004). The actual load transfer to the SWCNTs observed in this study falls short of the 100% transfer. This is likely due to the presence of CNT clusters, nanotube bundles, and low interfacial strength between nanotube and matrix. Liao and Li (2001) suggested that the most likely method of load transfer between polymer matrix and CNTs is by a combination of van der Waals and electrostatic forces as well as mechanical interlocking via mismatch in coefficients of thermal expansion between CNTs and the polymer matrix. There is very little evidence that strong bonds exist in purified SWCNTs that would allow greater load transfer. It is believed that in the case of nanotube bundles, the polymer matrix can actually infiltrate the bundle, interlocking with individual nanotubes (Schadler, Giannaris, & Ajayan, 1998) thus allowing load transfer to inner nanotubes within the bundle. It is likely that this effect is limited and it should not be assumed that all bundles are fully infiltrated with polymer matrix. Nanotubes that are located towards the center of bundles are likely to slip at lower composite strains. This is plausible since the shear strength is lower for the nanotube/nanotube interface than the nanotube/phenolic resin interface. The limited load transfer presented in Figure 23 and SWCNT bundles and clusters observed by optical micrographs presented in Figure 14 through Figure 17 and SEM presented in Figure 18 through Figure 21, confirms this.

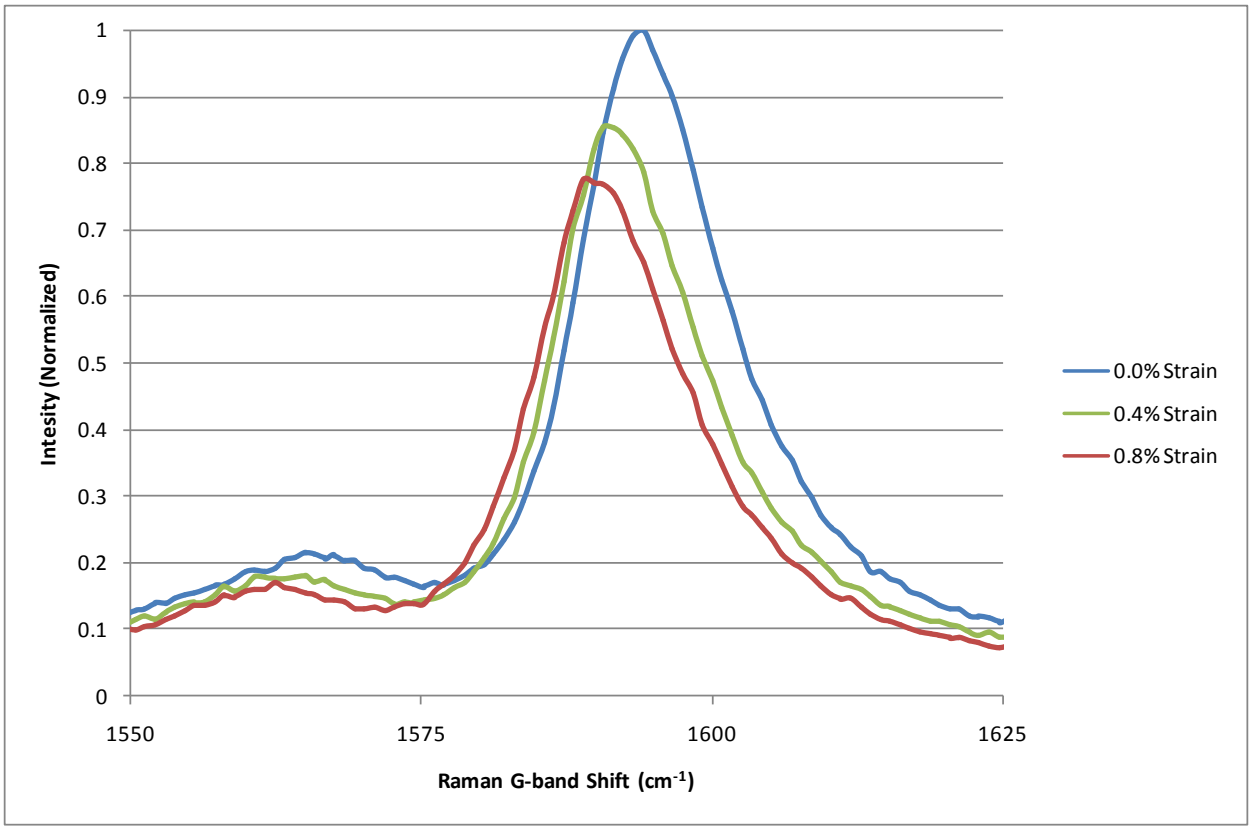

Figure 22: Raman spectra of the G-band for 0.25 wt % SWCNT composite at various tensile strains.

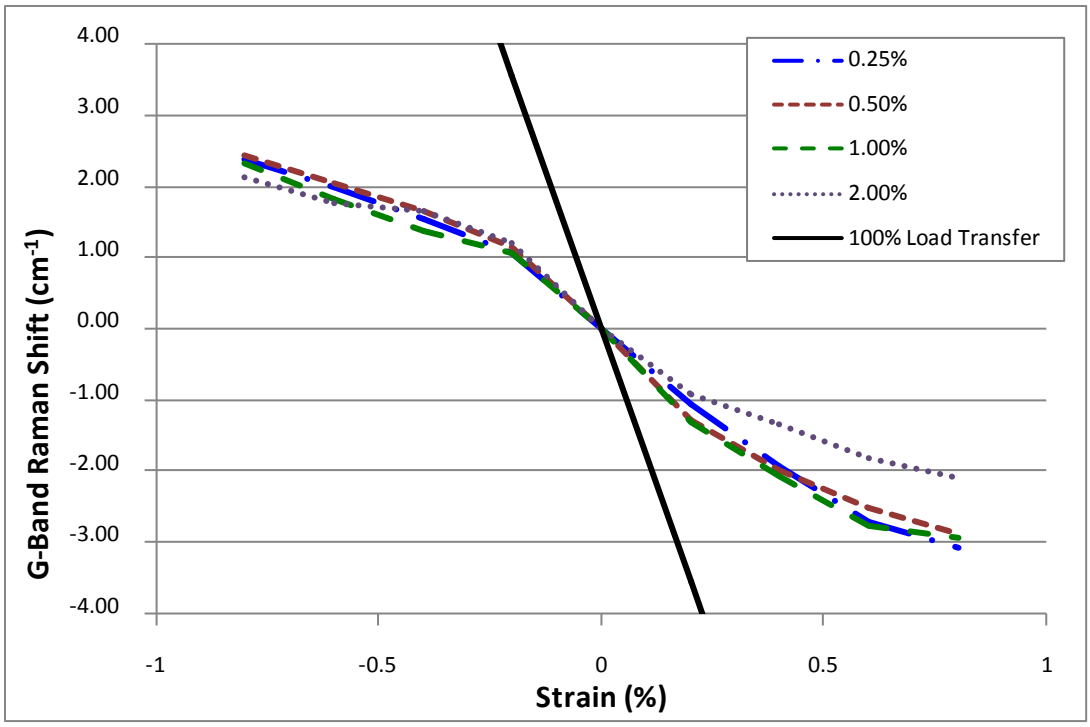

Figure 23: Average G-band shift of composite with varying amounts of SWCNTs as a function of strain ranging from -0.8% to 0.8%. The solid line represents 100% load transfer.

Figure 24 shows the total Raman G^+ peak down-shift due to 0.8% tensile strain for composites with varying concentrations of SWCNTs, based on ten measurement locations. This was calculated by the difference between the Raman shift at zero strain and the Raman shift at 0.8% strain. There is a decline in the total down-shift observed at higher concentrations. This means that the efficiency of load transfer decreases as the SWCNT concentration increases. A main decrease in load transfer appears to occur when the SWCNT concentration exceeds 1.00%. This finding is also observable in Figure 23; the load transfer results are similar for the 0.25%, 0.50% and 1.00% CNT composites but much lower for the 2.00% CNT composite. Since load transfer efficiency would be the highest for well-bonded and well-dispersed SWCNTs, any reduction in

dispersion, which further can deteriorate the interfacial bonding between SWCNTs and phenolic resin, is unfavorable for load transfer. Difficulty in dispersion of SWCNTs at higher loading has been observed by optical micrographs presented in Figure 14 through Figure 17 and SEM presented in Figure 18 through Figure 21. A decrease in load transfer efficiency of SWCNTs at higher concentrations is attributed to the reduction in dispersion.

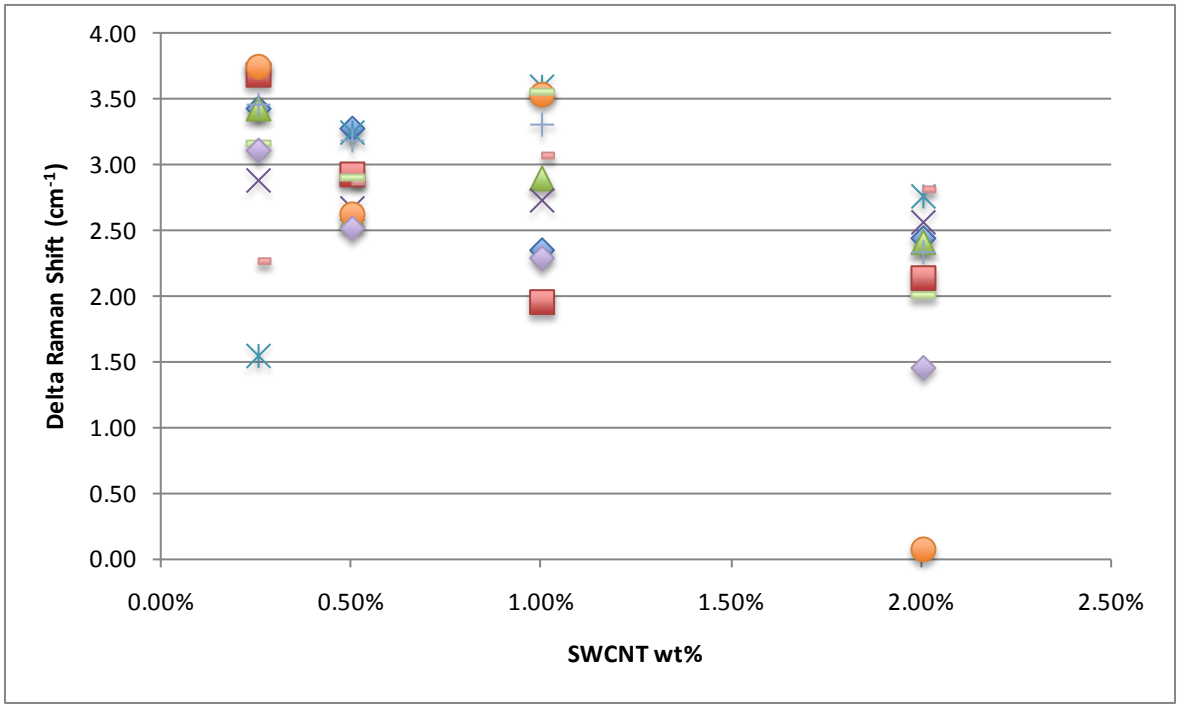

Figure 24: Total change in G^+ peak shifts measured at 10 locations within the composites with varying SWCNT concentration due to total tensile strain of 0.8%.

Figure 25 shows the total Raman G^+ peak up-shift due to -0.8% compressive strain for composites with varying concentrations of SWCNTs, based on ten measurement locations. This

was calculated by the difference between the Raman G^+ peak at zero strain and the Raman G^+ peak at -0.8% strain. There is no noticeable change in the total up-shift as a function of SWCNT concentration. This implies that the SWCNT concentration has little effect on the efficiency of load transfer under compressive strain. This result agrees with Schadler, Giannaris, & Ajayan (1998), who suggested that in compression, slippage of CNTs does not occur due to geometrical constraints. Therefore the load transfer efficiency remains the same regardless of SWCNT concentration or degree of dispersion.

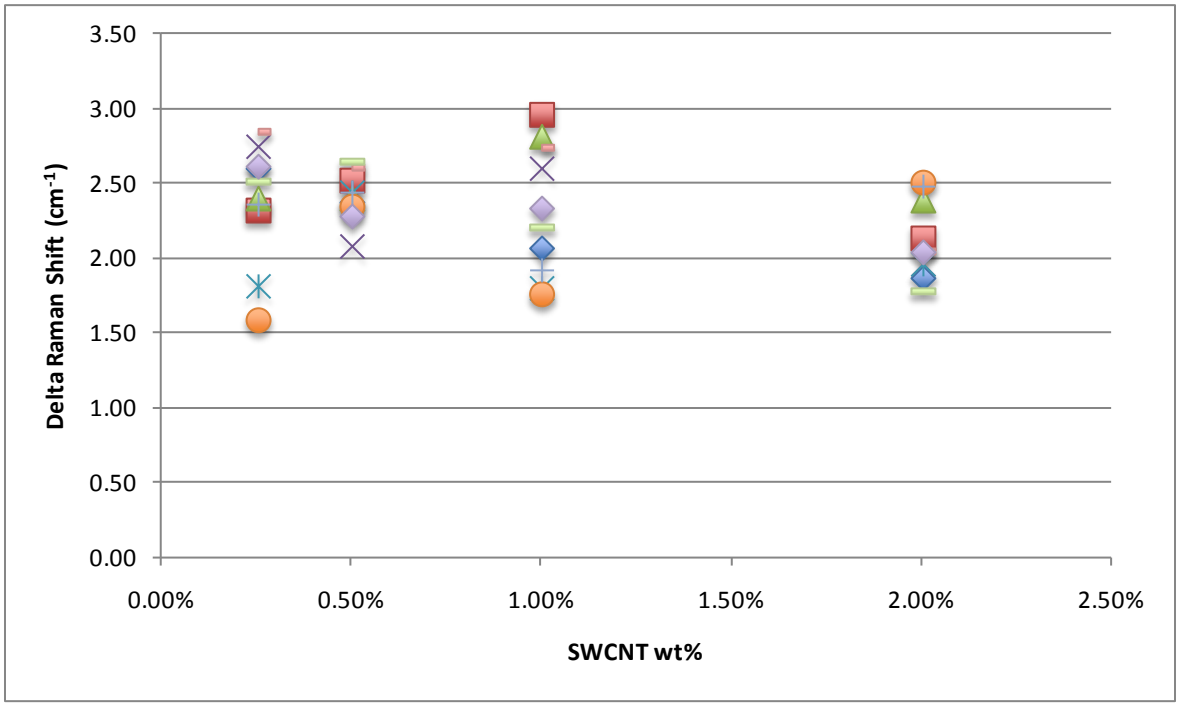

Figure 25: Total change in G^+ peak shifts measured at 10 locations within the composites with varying SWCNT concentration due to total compressive strain of -0.8%.

Figure 26 shows the slope (cm^{-1}/% strain) of the Raman shift as a function of SWCNT concentration at low compressive and tensile strains (-0.2% to 0.2%). The slope remains relatively constant, independent of SWCNT concentration. At very low strains, slip between SWCNTs and SWCNT/phenolic resin would not occur, even in tension. Therefore, the load transfer efficiency remains the same.

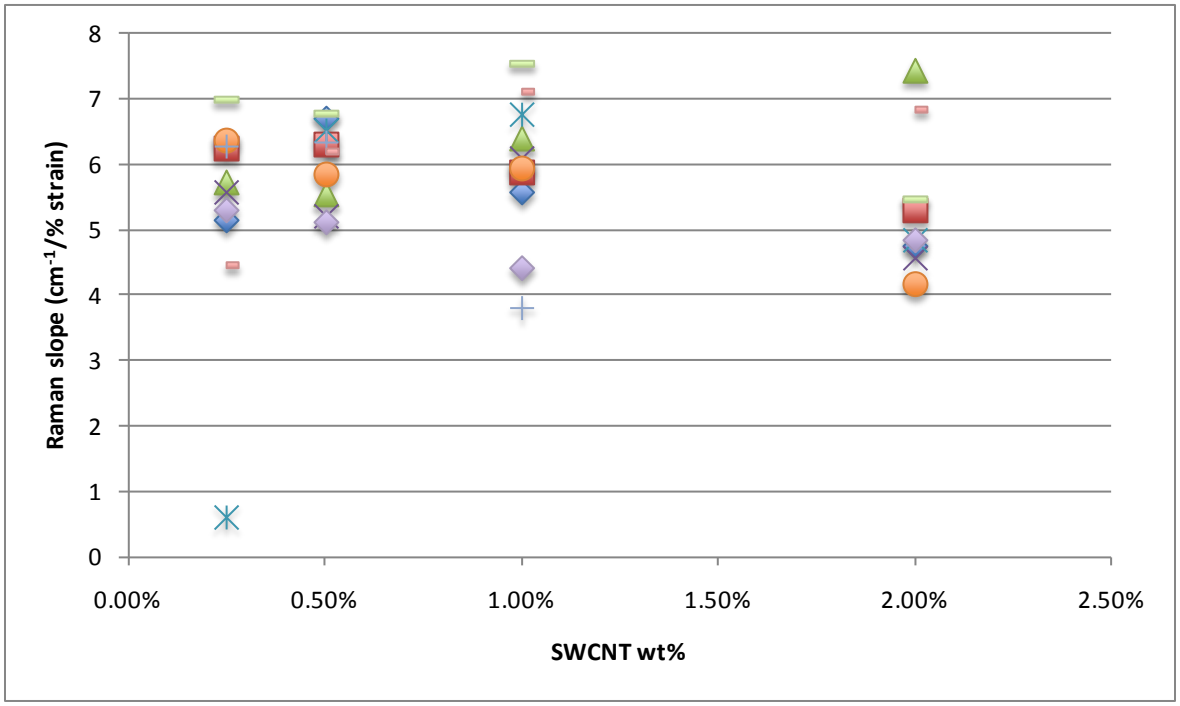

Figure 26: Slope of the G^+ peak shifts measured at 10 locations within the composites with varying SWCNT concentration at small strains from -0.2% to 0.2%.

4.2.4 Summary of Purified SWCNT/Phenolic Resin Composite

Optical and scanning electron microscopy revealed that poor dispersion of SWCNTs occurred with an increase in their concentration in SWCNT/phenolic resin composite. The load transfer efficiency in total tension (0.8%) decreases with an increase in concentration of SWCNTs. This is due to the fact that the degree of dispersion decreases at higher concentrations of SWCNTs, decreasing the total SWCNT/phenolic resin interfacial surface area, which gives rise to slippage of SWCNTs that do not interface with phenolic resin. On the contrary, in compression, interfacial slippage from poorly dispersed SWCNTs is limited by geometrical constraints. This results in constant load transfer efficiency independent of CNT concentrations. However, at very low strain (± 0.2%) load transfer efficiency remains constant regardless of SWCNT concentration in both tension and compression. This further confirms the influence of slippage and poor dispersion on load transfer efficiency.

4.3 Characterization of Functionalized SWCNTs

Purified HiPco SWCNTs were functionalized using the process described in 3.1.3, which is expected to improve dispersibility of the CNTs in phenolic resin. Characterization was performed to verify that the SWCNTs were properly functionalized with phenyl sulfonate molecules. The characterization techniques used to evaluate the degree of functionalization were Raman and XPS.

4.3.1 Raman

Figure 27 shows the Raman spectra of the phenyl sulfonated SWCNTs. The intensity of the D-band has increased significantly when compared with the purified SWCNTs, shown in Figure 2. The increase in D-band intensity signifies disorder in SWCNTs, which is triggered by the surface modification incurred during the phenyl sulfonation of the SWCNTs. The average D/G intensity ratio of three samples of phenyl sulfonated SWCNTs is 0.330 with a standard deviation of 0.014. This is consistent with previous results obtained from functionalized SWCNTs, as shown in Figure 28. However, it cannot be positively concluded that an increase in disorder is entirely due to the attachment of the phenyl sulfonate groups. Damage to the nanotubes or unattached contaminants could also cause an increase in the D-band intensity.

The D-band and G-band locations are consistent with previous phenyl sulfonated SWCNTs as shown in Figure 28. The average G-band position of the three samples is 1594.84 cm^{-1} with a standard deviation of 0.855 cm^{-1} and the D-band position is 1296.78 cm^{-1} with a standard deviation of 1.385 cm^{-1}. This is consistent with previous results (P. Nikolaev, personal communication, November 2008) obtained from functionalized SWCNTs as shown in Figure 28.

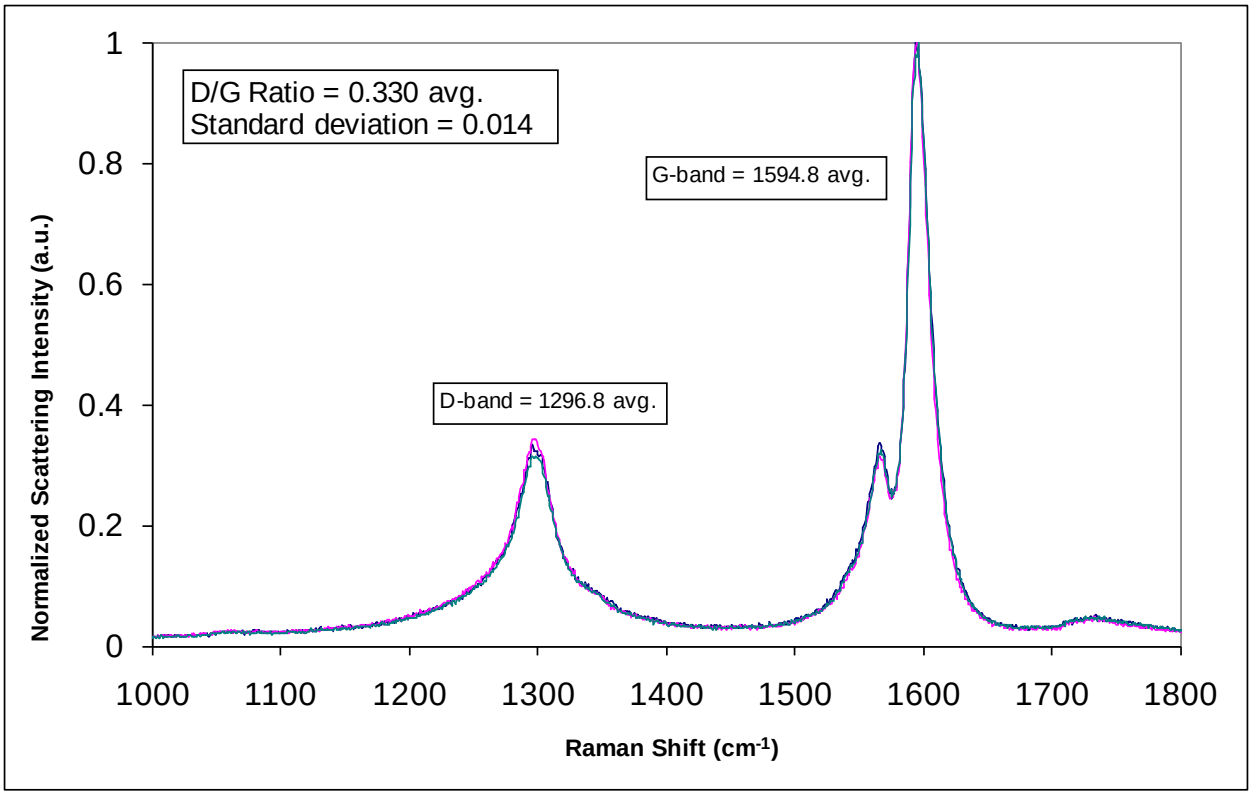

Figure 27: Raman spectra of phenyl sulfonated SWCNTs localized at the G-band region.

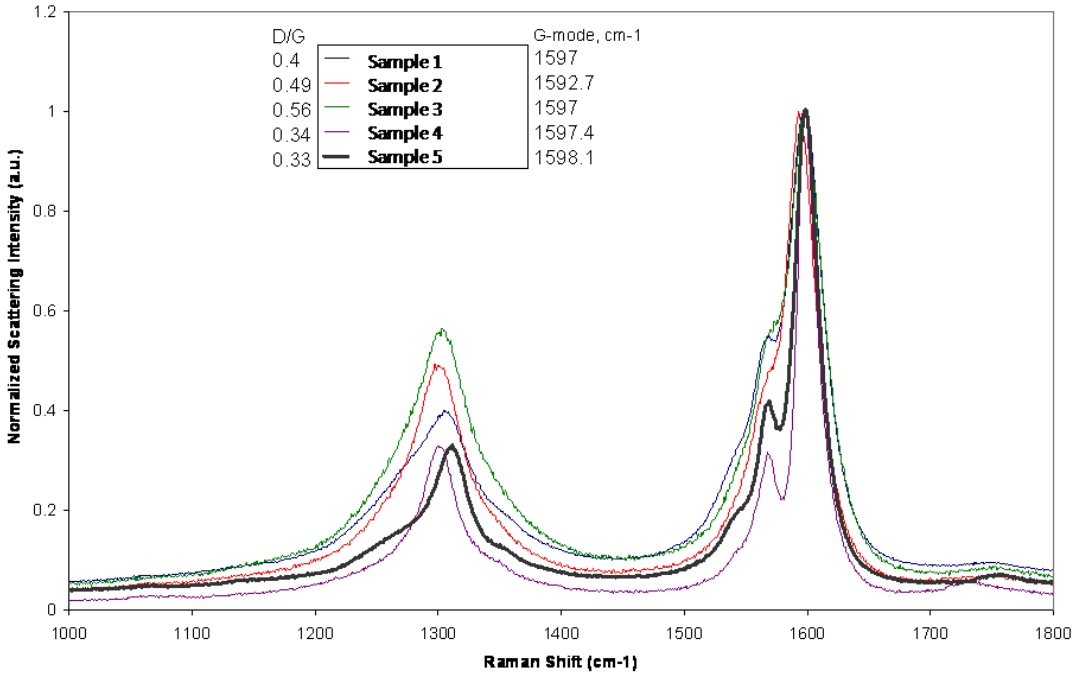

Figure 28: Typical Raman spectra of phenyl sulfonated SWCNTs produced and characterized at NASA-JSC (Data provided by Edward Sosa).

4.3.2 XPS

X-ray photoelectron spectroscopy (XPS) can help determine the degree of functionalization of SWCNTs by examining the elemental composition and electronic state near the surface of the material. The spectra from three samples are shown in Figure 29 through Figure 31. They showed peaks corresponding to carbon, oxygen, sulfur, calcium and indium. Peaks from carbon, oxygen and sulfur originate from carbon nanotubes with R-SO_3 functions. The indium peaks come from the indium foil, on the specimen holder. The calcium peaks, however, are of concern.

Quantitative analysis indicated that the ratio of oxygen to sulfur was higher than expected for R-SO_3 functions. This implies that not all oxygen is engaged in forming the R-SO_3 functions.

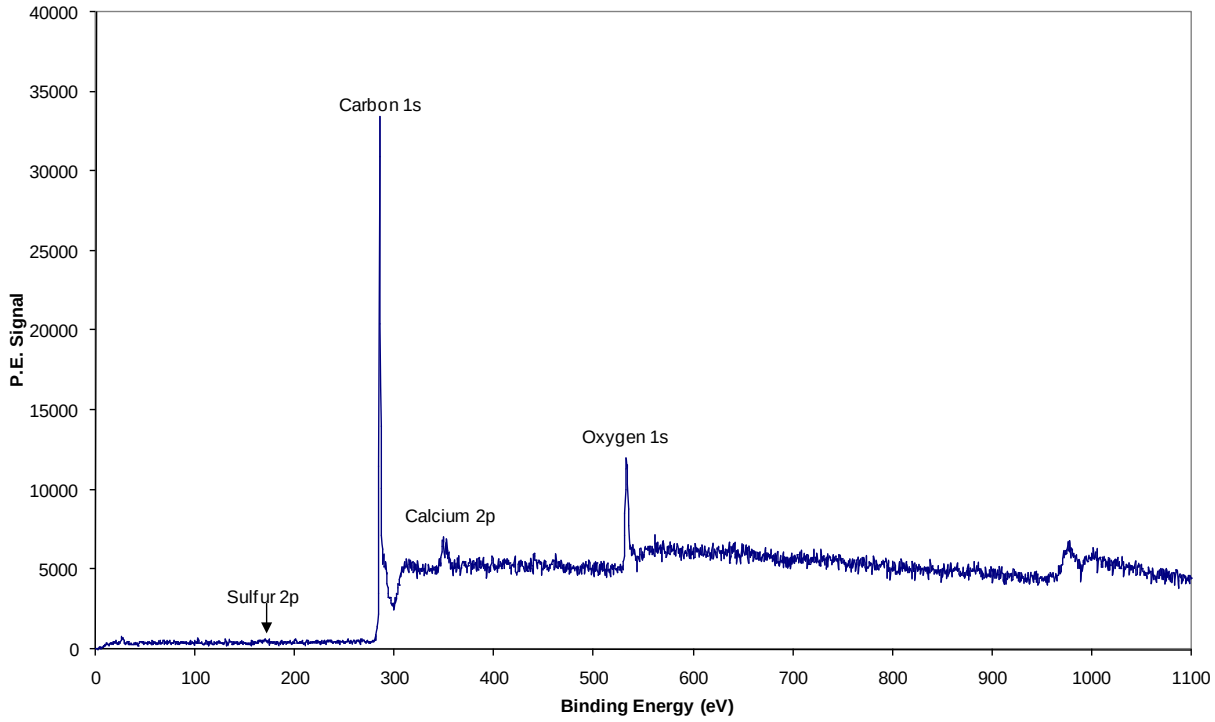

Figure 29: XPS data of phenyl sulfonated SWCNTs, sample 1.

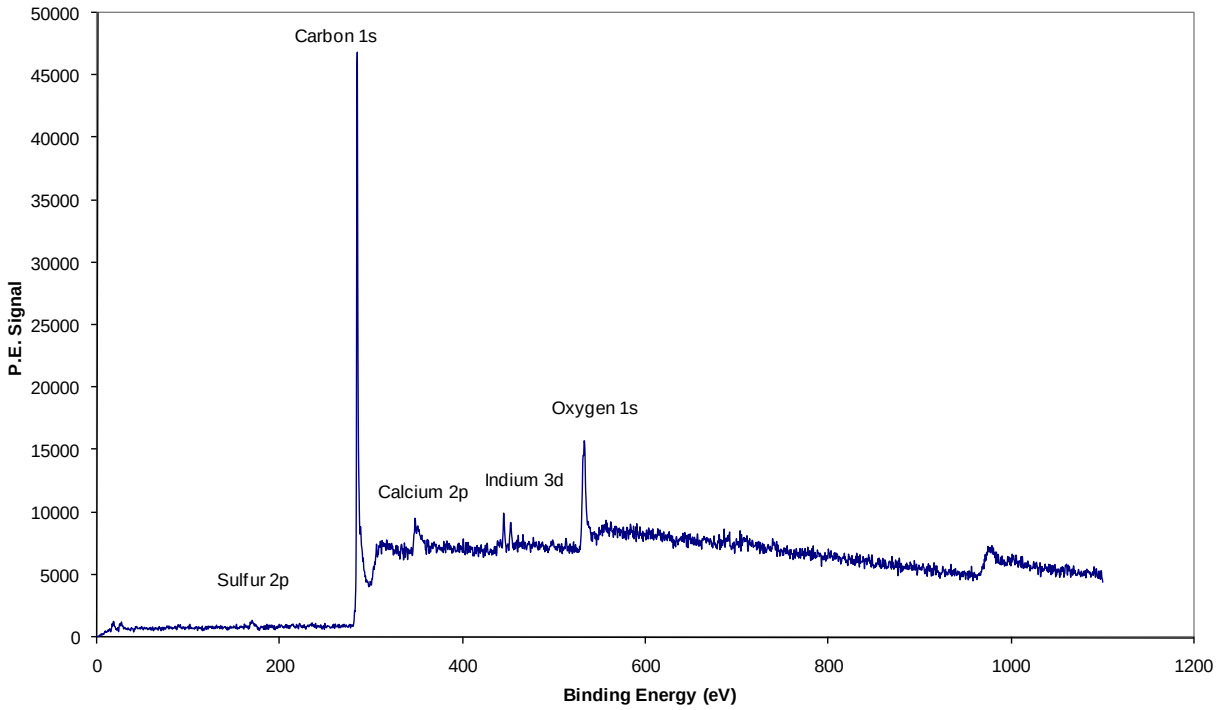

Figure 30: XPS data of phenyl sulfonated SWCNTs, sample 2.

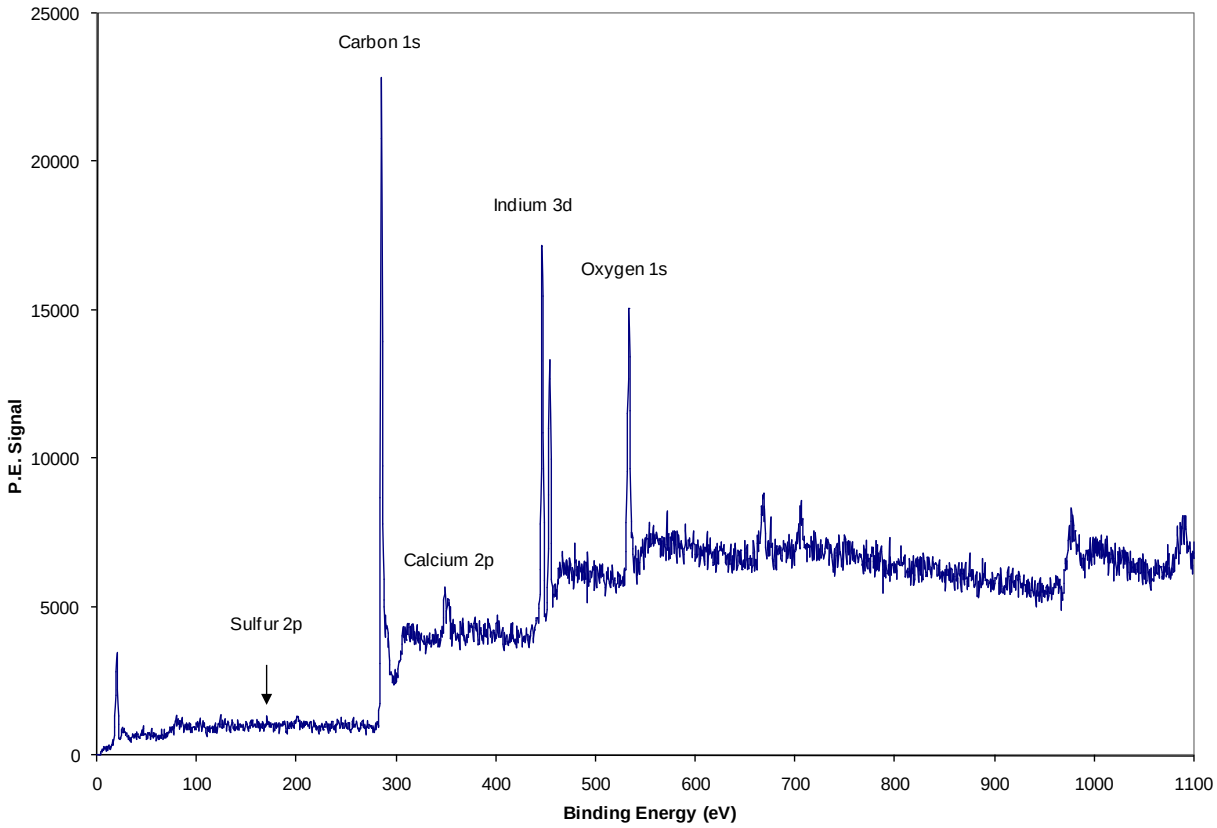

Figure 31: XPS data of phenyl sulfonated SWCNTs, sample 3.

Figure 32 shows the localized spectrum for the carbon peak, located at approximately 285 eV, which represents the carbon in SWCNTs and phenyl groups. The peak has a broad shoulder near the base at approximately 287 eV. This is typically due to small amounts of oxidation of the SWCNTs and potentially carbon dioxide that has been adsorbed on the surface of the SWCNTs. Sulfuric acid used in the phenyl sulfonation process may have caused a small amount of oxidation of the nanotubes into carbonyls, which have a slightly higher binding energy than carbon, causing this shoulder (Moulder, Stickle, Sobol, & Bomben, 1995).

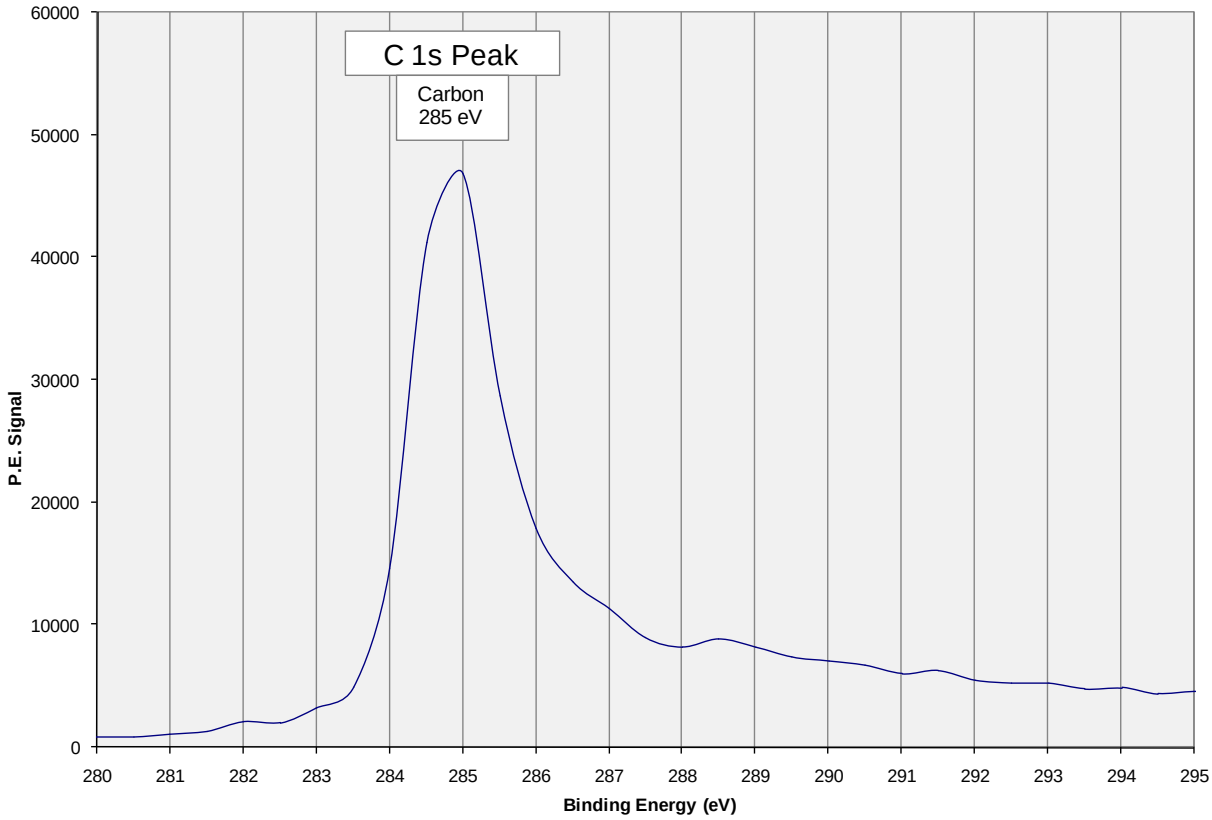

Figure 32: XPS data for carbon peak from phenyl sulfonated SWCNTs.

Figure 33 shows the localized spectrum of sulfur peaks consisting of the $2p_{3/2}$ and the higher $2p_{1/2}$, which corresponds to sulfur oxides, including sulfite (SO_3^{2-}) and sulfate (SO_4^{2-}) (Moulder, Stickle, Sobol, & Bomben, 1995). The sulfite peak likely represents the sulfonate groups that are present as functional groups; however, the intensity of the peaks suggests that there is a higher content of sulfur in the form of sulfate. This cannot be attributed to the phenyl sulfonate functional group, and therefore implies that there is a reaction product containing sulfur and contaminants, which deterred a portion of the sulfur from forming sulfonate groups. Given the

proper functionalization, the sulfur peak would be stronger and consist of only the sulfite peak. Therefore, the sulfite peak, relative to the carbon peak in these samples, is weak (E. D. Sosa, personal communication, December 2008). This corresponds to very little sulfonate molecules in the SWCNTs.

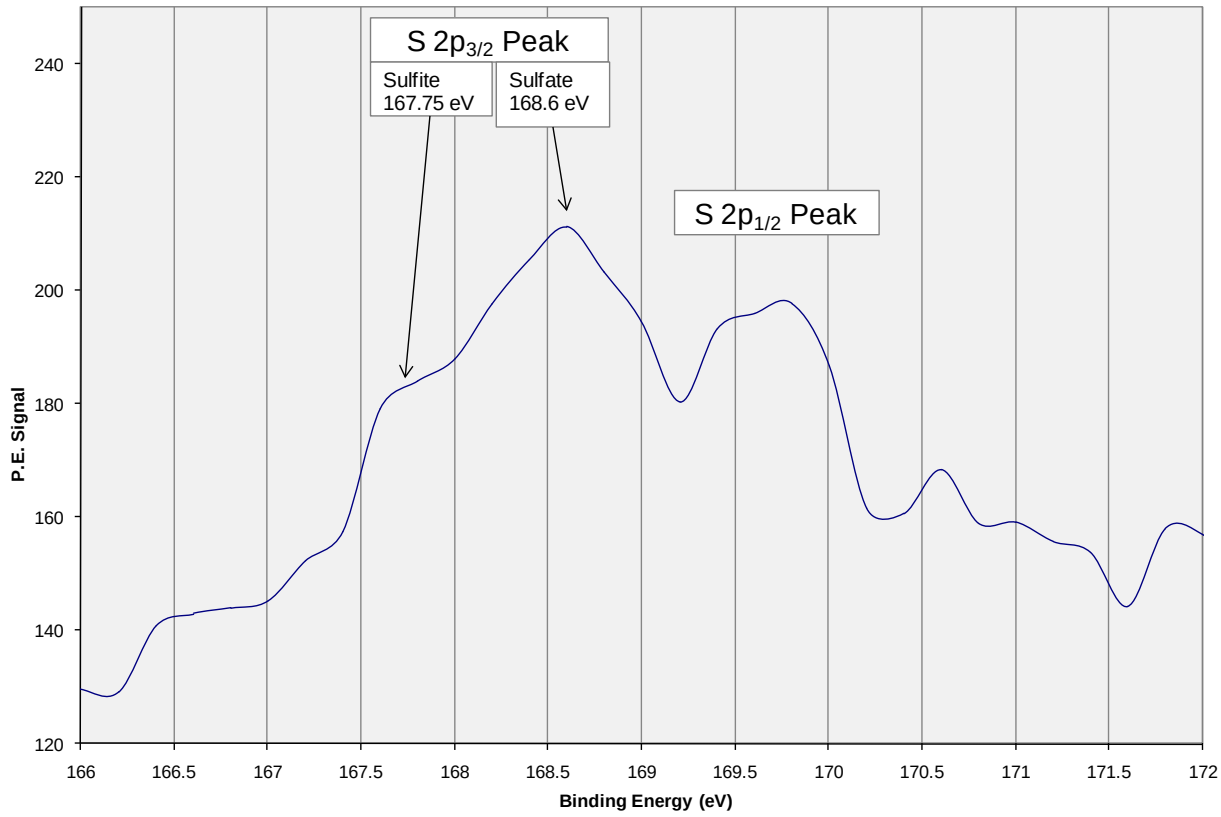

Figure 33: XPS data for sulfur peak from phenyl sulfonated SWCNTs.

The localized spectrum of oxygen, presented in Figure 34, shows an asymmetric shape and large width, indicating that multiple oxides may be present. The prominent peak is located at

approximately 532 eV, typical of sulfates (Moulder, Stickle, Sobol, & Bomben, 1995). However, given the asymmetric shape and large width, other oxides such as carbonyls that result from oxidation of CNTs and adsorbed water vapor may exist.

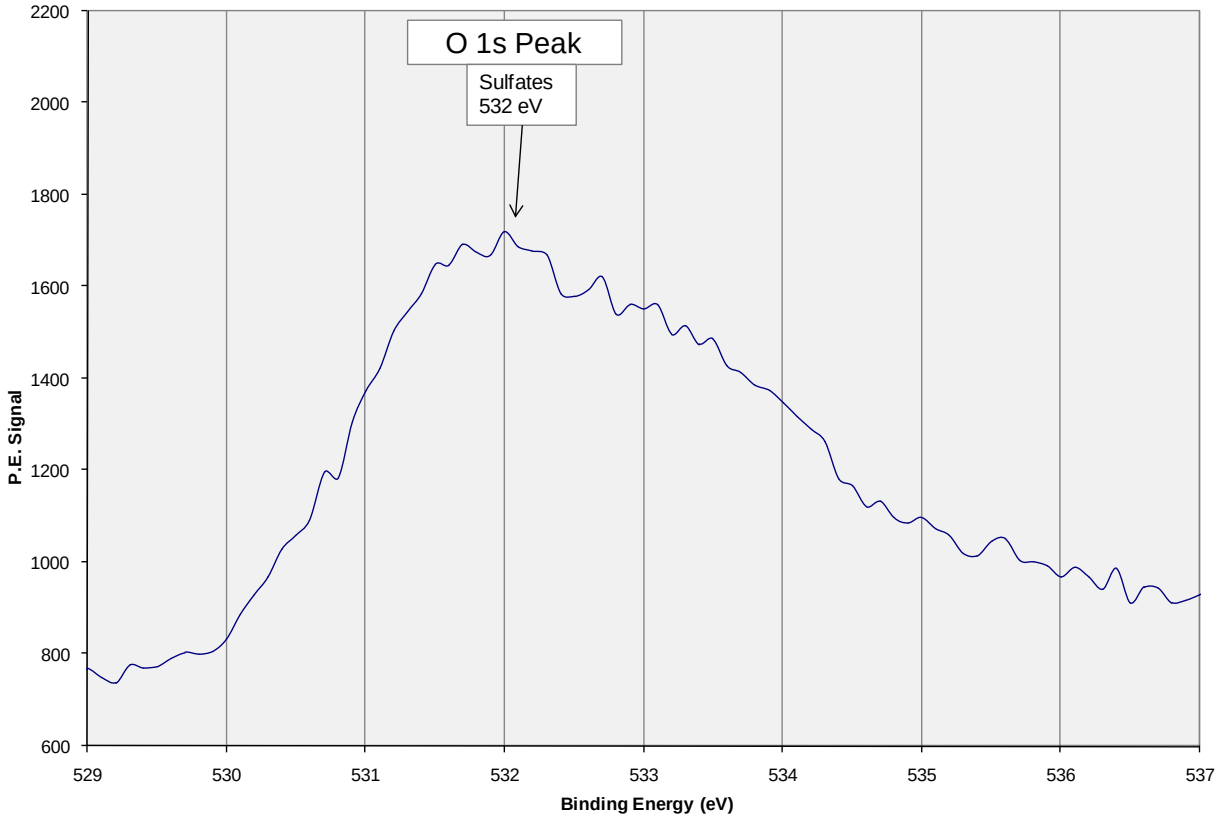

Figure 34: XPS data for oxygen peak from phenyl sulfonated SWCNTs.

The localized spectrum of the calcium peak shows both the $2p_{3/2}$ peak and the higher energy $2p_{1/2}$ peak of the calcium. The $2p_{3/2}$ peak occurs at approximately 348.5 eV, which corresponds to calcium sulfate, $CaSO_4$ (Moulder, Stickle, Sobol, & Bomben, 1995). This result coincides with

the oxygen and sulfur peaks, which indicate the presence of sulfur and oxygen in the form of SO_4. This concludes that the sulfate and calcium found are in the form of calcium sulfate ($CaSO_4$). The formation of calcium sulfate is likely initiated by contamination during the functionalization process. Contaminated glassware or deionized water may have been the source of the calcium contamination.

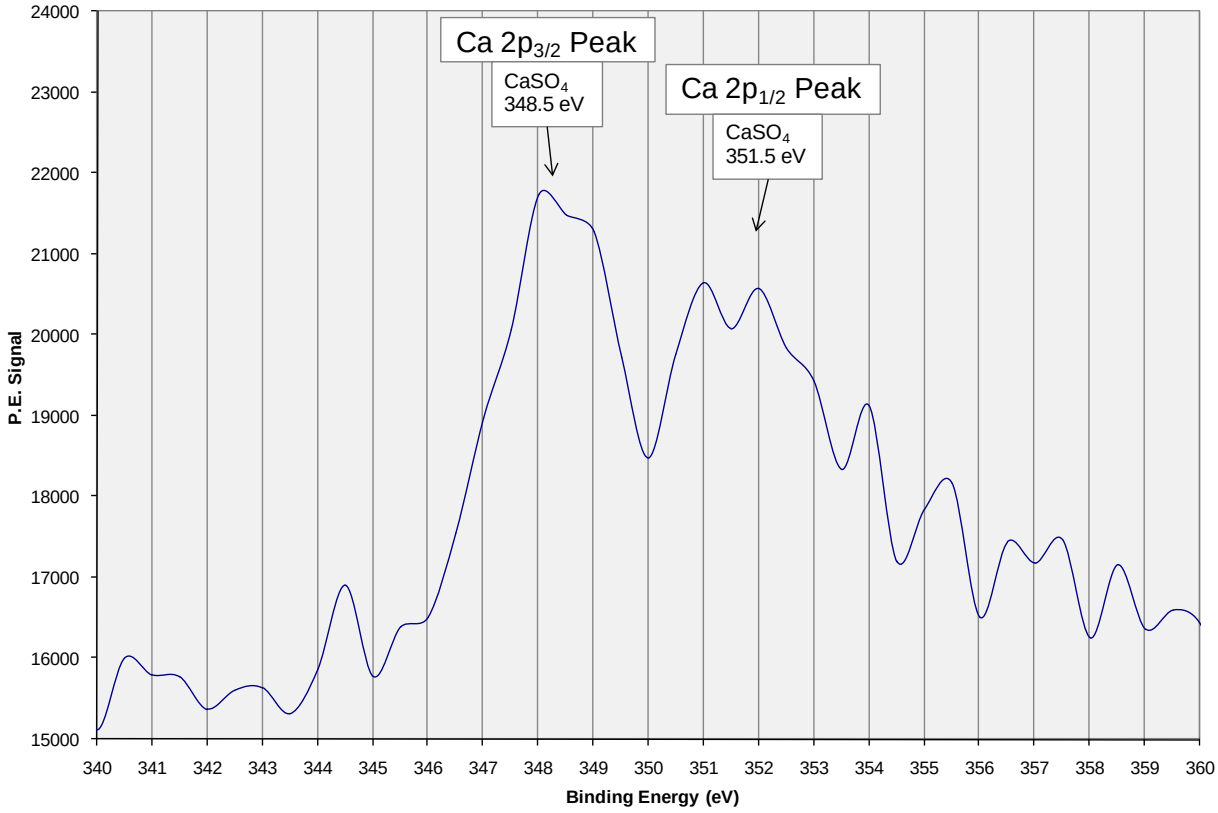

Figure 35: XPS data for calcium peak from phenyl sulfonated SWCNTs.

XPS results suggest that the phenyl sulfonated SWCNTs were contaminated with calcium. The SWCNTs contain a small amount of sulfonate, as well as calcium sulfate impurity. Even if all the sulfur detected in the sulfite is entirely functionalized on the phenylated SWCNTs as a sulfonate group, the degree of functionalization is lower than typical phenyl sulfonated nanotubes. Functionalization may have been hindered by the calcium contamination during the reaction by deterring a portion of the sulfur from forming sulfonate groups.

4.3.3 Summary of Functionalized SWCNTs Characterization

Characterization of the phenyl sulfonated SWCNTs indicated that calcium was introduced as a contaminant that inhibited functionalization of the SWCNTs.

4.4 Analysis of Functionalized SWCNT/Phenolic Resin Composite

The functionalized SWCNTs were also evaluated for their ability to form a composite with phenolic resin matrix. Two composite test coupons were fabricated using the method described in section 3.2. These coupons were examined by optical microscopy for uncured composite and macroscopically for the cured composite.

4.4.1 Optical Microscopy of Uncured Composite

Figure 36 shows the optical micrographs from uncured composite fabricated with 0.0625 wt% of (a) phenyl sulfonated nanotubes and (b) purified nanotubes. These micrographs show the dispersion of CNTs in the ethylene glycol and phenolic resin prior to cure. The dark gray areas correspond to dispersed SWCNT bundles. The black spots represent tightly bound clusters of

SWCNT bundles, which likely will not be infiltrated with phenolic resin, and will not help to improve the strength of the composite. For the composite fabricated with purified SWCNTs, there is a larger amount of dark gray areas that correspond to dispersed SWCNT bundles. Overall, the phenyl sulfonated SWCNTs were not as well dispersed as the purified HiPco SWCNTs.

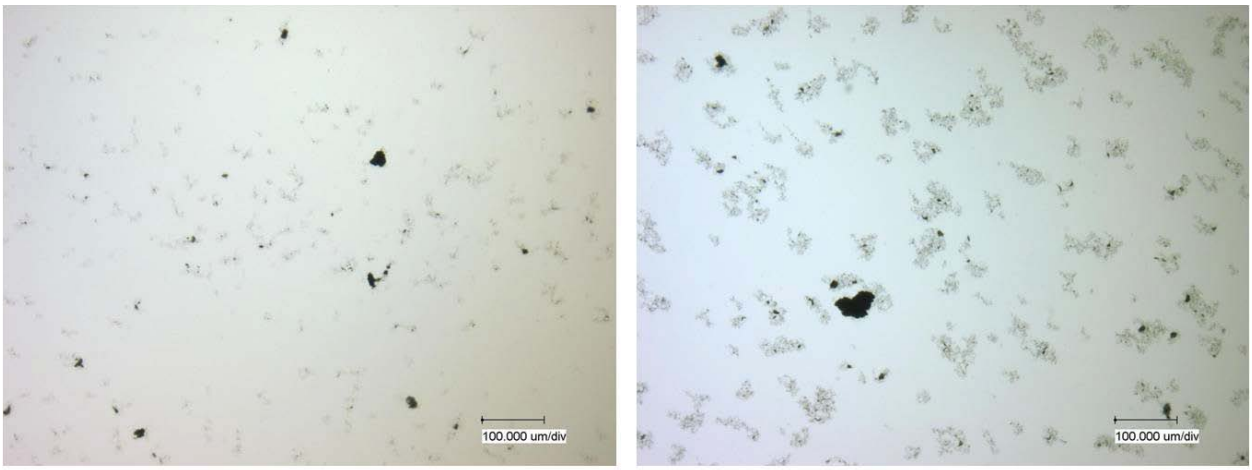

Figure 36: Optical micrograph of composite prior to cure with: (a) 0.0625 wt% phenyl sulfonated SWCNTs and (b) 0.0625 wt% purified HiPco SWCNTs.

4.4.2 Macroscopic Analysis of Composite

Typical macroscopic photographs from composite coupons fabricated using (a) phenyl sulfonated and (b) purified SWCNTs at 0.0625 wt% is presented in Figure 37. A clear inhomogeneity in the composite fabricated with phenyl sulfonated SWCNTs is observed by transparent yellow matrix and regions of opaque black (SWCNTs in phenolic resin). After curing, the composite would contain microscopic clusters of SWCNTs up to approximately

25µm in size as shown in Figure 36. However, a large-scale inhomogeneity, such as that shown in Figure 37(a), suggests that a proper functionalization is critical to fabricate composites with structural integrity. Results from this study demonstrate that the dispersibility of the phenyl sulfonated SWCNTs, which contain a small amount of sulfonate, as well as calcium sulfate impurity, is worse than that of the purified SWCNTs. The composite fabricated from 0.0625 wt% purified HiPco SWCNTs was clearly more homogeneous, as shown in Figure 37(b). Higher concentrations of purified SWCNTs are required in order to disperse the SWCNTs into the entire volume of the matrix.

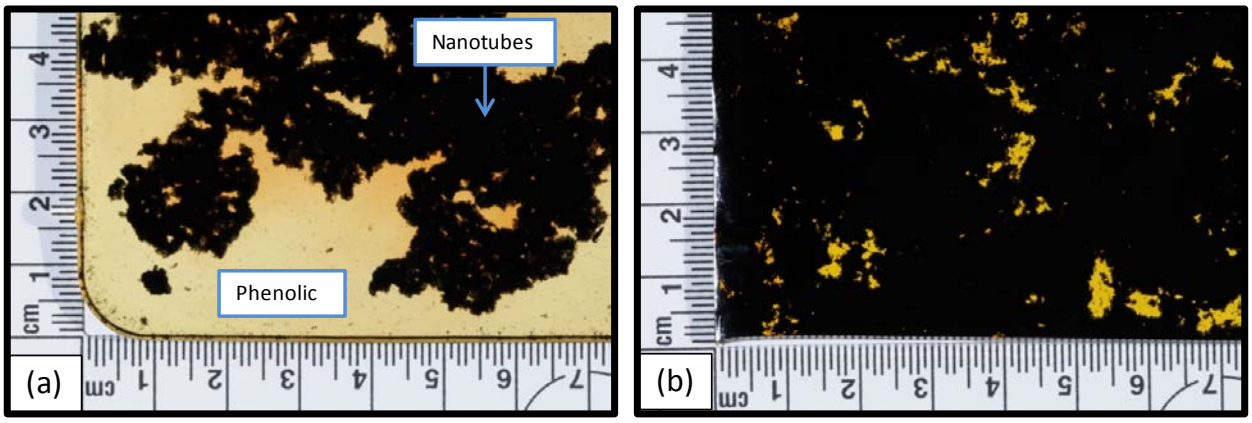

Figure 37: Macroscopic photographs of cured composite with: (a) 0.0625 wt% phenyl sulfonated SWCNTs and (b) 0.0625 wt% purified HiPco SWCNTs.

4.4.3 Summary of Functionalized SWCNT/Phenolic Resin Composite

The use of contaminated phenyl sulfonated SWCNTs resulted in macroscopic inhomogeneity within the composite that could not be further evaluated. A proper functionalization of SWCNTs appears to be critical in successful fabrication of SWCNT reinforced phenolic resin composite.

5 CONCLUSIONS

In this investigation, purified and phenol sulfonated SWCNTs were examined as reinforcements in phenolic resin composites. Specifically, a detailed study was carried out to characterize purified and phenol sulfonated SWCNTs. Microscopic and macroscopic homogeneity in composites were also examined. For phenolic resin composite reinforced with purified SWCNTs, load transfer efficiency of SWCNTs was determined with respect to concentration and magnitude of strain. For the composite with phenyl sulfonated SWCNTs, amount of sulfonate and the presence of calcium sulfate impurities were observed to be critical for microscopic and macroscopic homogeneity. Details of the findings from this study include:

- The purified HiPco SWCNTs were determined to be sufficiently purified for composite fabrication with phenolic resin matrix.
- Prior to curing, clustering of SWCNT bundles was observed to increase with an increase in concentration of SWCNTs in the composite.
- Load is transferred from the phenolic resin to purified SWCNTs during strain events on the composite. This demonstrates the potential to strengthen phenolic resin composites, reinforced with SWCNTs.
- The load transfer efficiency in total tension (0.8%) decreased with an increase in concentration of SWCNTs. On the contrary, in total compression (-0.8%), the load transfer efficiency remained constant as a function of SWCNT concentration.

- At very low strain (± 0.2%) the load transfer efficiency remains constant regardless of SWCNT concentration in both tension and compression.
- Characterization of the phenyl sulfonated SWCNTs indicated that calcium was introduced as a contaminant that interfered with functionalization of the SWCNTs. The use of contaminated phenyl sulfonated SWCNTs resulted in macroscopic inhomogeneity within the composite. Proper functionalization of SWCNTs appears to be critical in successful fabrication of SWCNT reinforced phenolic resin composite.

LIST OF REFERENCES

Arepalli, S., Nikolaev, P., Gorel, O., Hadjiev, V. G., Holmes, W., Files, B., et al. (2004). Protocol for the characterization of single-wall carbon nanotube material quality. *Carbon , 42*, pp. 1783 - 1791.

Boul, P. (2008). Unbublished Research.

Chiang, I. W., Brinson, B. E., Huang, A. Y., Willis, P. A., Bronikowski, M. J., Margrave, J. L., et al. (2001). Purification and Characterization of Single-Wall Carbon Nanotubes (SWNTs) Obtained from the Gas-Phase Decomposition of CO (HiPco Process). *J. Phys. Chem.* , 8297-8301.

Coleman, J. N., Cadek, M., Ryan, K. P., Fonseca, A., Nagy, J. B., Blau, W. J., et al. (2006). Reinforcement of polymers with carbon nanotubes. The role of an ordered polymer interfacial region. Experiment and modeling. *Polymer , 47*, 8556-8561.

Coleman, J. N., Khan, U., Blau, W. J., & Gun'ko, Y. K. (2006). Small but strong: A review of the mechanical properties of carbon nanotube–polymer composites. *Carbon , Vol. 44* (no. 9), pp. 1624 - 1652.

Cronin, S. B., Swan, A. K., Unlu, M. S., Goldberg, B. B., Dresselhaus, M. S., & Tinkham, M. (2004). Measuring the Uniaxial Strain of Individual Single-Wall Carbon Nanotubes: Resonance Raman Spectra of Atomic-Force-Microscope Modified Single-Wall Nanotubes. *Physical Review Letters , 93* (16).

Ding, W., Eitan, A., Fisher, F. T., Chen, X., Dikin, D. A., Andrews, R., et al. (2003). Direct observation of polymer sheathing in carbon nanotube-polycarbonate composites. *Nano Letters , 3* (11), 1593-1597.

Dresselhaus, M. S., & Avouris, P. (2001). *Carbon Nanotubes: Synthesis, Structure, Properties, and Applications.* (M. S. Dresselhaus, G. Dresselhaus, & P. Avouris, Eds.) New York: Springer.

Dresselhaus, M. S., Dresselhaus, G., Saito, R., & Jorio, A. (2005). Raman spectroscopy of carbon nanotubes. *Physics Reports , 409* (2), 47-99.

Du, C., Yeh, J., & Pan, N. (2005). High power density supercapacitors using locally aligned carbon nanotube electrodes. *Nanotechnology , 16*, 350-353.

Hata, K., Futaba, D. N., Mizuno, K., Namai, T., Yumura, M., & Iijima, S. (2004). Water-Assisted Highly Efficient Synthesis of Impurity-Free Single-Walled Carbon Nanotubes. *Science , 306* (5700), 1362 - 1364.

Huang, Y. Y., & Terentjev, E. M. (2008). Dispersion and rheology of carbon nanotubes in polymers. *The internation journal of material forming , 1*, 63-74.

Iijima, S. (1991). Helical microtubules of graphitic carbon. *Nature , 354*, 56-58.

Iijima, S., & Ichihashi, T. (1993). Single-shell carbon nanotubes of 1-nm diameter. *Nature , 363*, 603-605.

Jorio, A., Dresselhaus, M. S., & Dresselhaus, G. (Eds.). (2008). Carbon Nanotubes: Advanced Topics in the Synthesis, Structure, Properties and Applications. *Topics in Applied Physics , 111*.

Kumar, R. (2009). *Raman Spectroscopy of Carbon Nanotubes under Axial Strain.* Saarbrucken, Germany: VDM Verlag Dr. Müller.

Liao, K., & Li, S. (2001). Interfacial characteristics of a carbon nanotube–polystyrene composite system. *Applied Physics Letters , 79* (25), 4225-4227.

Lin, Y., Zhou, B., Fernando, K. S., Liu, P., Allard, L. F., & Sun, Y.-P. (2003). Polymeric Carbon Nanocomposites from Carbon Nanotubes Functionalized with Matrix Polymer. *Macromolecules , 36* (19), 7199-7204.

Liu, Z., Sun, X., Nakayama-Ratchford, N., & Dai, H. (2007). Supramolecular Chemistry on Water-Soluble Carbon Nanotubes for Drug Loading and Delivery. *ACSNano , 1* (1), 50-56.

López Manchado, M. A., Valentini, L., Biagiotti, J., & Kenny, J. M. (2005). Thermal and mechanical properties of single-walled carbon nanotubes–polypropylene composites prepared by melt processing. *Carbon , Vol. 43* (no. 7), pp. 1499 - 1505.

Martinez, M. T., Callejas, M. A., Benito, A. M., Cochet, M., Seeger, T., Anson, A., et al. (2003). Sensitivity of single wall carbon nanotubes to oxidative processing: structural modification intercalation and functionalisation. *Carbon , 41*, 2247-2256.

Moulder, J. F., Stickle, W. F., Sobol, P. E., & Bomben, K. D. (1995). *Handbook of X Ray Photoelectron Spectroscopy.* Physical Electronics.

Nikolaev, P. (2004). Gas-Phase Production of Single-Walled Carbon Nanotubes from Carbon Monoxide: Review of the HiPco Process. *JOURNAL OF NANOSCIENCE AND NANOTECHNOLOGY , 4* (4), 1-10.

Obraztsov, A. N., Pavlovsky, I., Volkov, A. P., Obraztsova, E. D., Chuvilin, A. L., & Kuznetsov, V. L. (2000). Aligned carbon nanotube films for cold cathode applications. *The journal of vacuum science and technology* , 1059-1063.

Potschke, P., Fornes, T. D., & Paul, D. R. (2002). Rheological behavior of multiwalled carbon nanotube/polycarbonate composites. *Polymer , 43*, 3247-3255.

Ryan, K. P., Cadek, M., Nicolosi, V., Blond, D., Ruether, M., Armstrong, G., et al. (2007). Carbon nanotubes for reinforcement of plastics? A case study with poly(vinyl alcohol). *Composites Science and Technology , 67*, 1640-1649.

Saito, R., Fantini, C., & Jiang, J. (2008). Excitonic States and Resonance Raman Spectroscopy of Single-Wall Carbon Nanotubes. In A. Jorio, M. S. Dresselhaus, & G. Dresselhaus, *Carbon Nanotubes: Advanced Topics in the Synthesis, Structure, Properties, and Applications* (pp. pp. 251 - 286). Springer.

Schadler, L. S., Giannaris, S. C., & Ajayan, P. M. (1998). Load transfer in carbon nanotube epoxy composites. *Applied Physics Letters , 73* (26), 3842-3844.

Tans, S. J., Devoret, M. H., Dai, H., Thess, A., Smalley, R. E., Geerligs, L. J., et al. (1997). Individual single-wall carbon nanotubes as quantum wires. *Nature , 386*, 474-477.

Terentjev, E. M. (2005). *Nematic Elastomer Nanocomposites as Electromechanical Actuators.*

Tran, H. K., Johnson, C. E., Rasky, D. J., Hui, F. C., Hsu, M.-T., Chen, T., et al. (1997). *Phenolic Impregnated Carbon Ablators (PICA) as Thermal Protection Systems for Discover Missions.* NASA Technical Memorandum 110440.

Vaisman, L., Wagner, H. D., & Marom, G. (2006). The role of surfactants in dispersion of carbon nanotubes. *Advances in Colloid and Interface Science* , 37-46.

Wang, Q. H., Setlur, A. A., Lauerhaas, J. M., Dai, J. Y., & Seelig, E. W. (1998). A nanotube-based field-emission flat panel display. *Applied Physics Letters* , 2912-2913.

Wei, B. Q., Vajtai, R., & Ajayan, P. M. (2001). Reliability and current carrying capacity of carbon nanotubes. *Applied Physics Letters , 79* (8), 1172-1174.

Wong, E. W., Sheehan, P. E., & Lieber, C. M. (1997). Nanobeam Mechanics: Elasticity, Strength, and Toughness of Nanorods and Nanotubes. *Science , Vol. 277* (no. 5334), pp. 1971 - 1975.

Yeh, M.-K., Tai, N.-H., & Liu, J.-H. (2006). Mechanical behavior of phenolic-based composites reinforced with multi-walled carbon nanotubes. *Carbon , 44*, 1-9.

Yu, M.-F., Lourie, O., Dyer, M. J., Moloni, K., Kelly, T. F., & Ruoff, R. S. (2000). Strength and Breaking Mechanism of Multiwalled Carbon Nanotubes Under Tensile Load. *Science , Vol. 287* (no. 5453), pp. 637 - 640.